

# Distortional analysis of simply supported box girders with inner diaphragms considering shear deformation of diaphragms using initial parameter method



Yangzhi Ren <sup>a,b,\*</sup>, Wenming Cheng <sup>b</sup>, Yuanqing Wang <sup>a</sup>, Qingrong Chen <sup>b</sup>, Bin Wang <sup>c</sup>

<sup>a</sup> Key Lab of Civil Engineering Safety and Durability of China Education Ministry, Department of Civil Engineering, Tsinghua University, Beijing 100084, China

<sup>b</sup> Department of Mechanical Engineering, Southwest Jiaotong University, No.111, North Section 1, Second Ring Road, Chengdu, Sichuan 610031, China

<sup>c</sup> College of Engineering, Design and Physical Sciences, Brunel University, London, Uxbridge UB8 3PH, UK

## ARTICLE INFO

### Article history:

Received 14 November 2016

Revised 27 April 2017

Accepted 3 May 2017

Available online 11 May 2017

### Keywords:

Simply supported girder

Diaphragm

Eccentric load

Shear deformation

Distortion

Initial parameter method

Finite element analysis

Experiment

Local stability

## ABSTRACT

In this paper, the distortion of simply supported girders with inner diaphragms subjected to concentrated eccentric loads is investigated using initial parameter method (IPM), in which the in-plane shear deformation of diaphragms is fully considered. A statically indeterminate structure was modeled with inner redundant forces, where the interactions between the girder and diaphragms were indicated by a distortional moment. Considering the compatibility condition between the girder and diaphragms, solutions for the distortional angle, warping displacements and stresses were derived and further simplified by establishing a matrix equation system. The validity of IPM was intensively verified by a finite element analysis and distortional experiments. Parametric studies were then performed to examine the effect of the diaphragm number on the distortional angle, warping displacements and stresses under various ratios of height to span of the girder and the diaphragm thicknesses. Besides, stabilities of the local web plate and mid-span diaphragm were analyzed based on IPM for box girders with symmetrical three inner diaphragms. Results show that the local web plate will buckle before overall yielding with the increment of the eccentric loads  $P_j$ , and the mid-span diaphragm is constantly stable in the whole deformation process. It shows that more attentions should be paid on the stability of the local web plate than overall yielding for girders subjected to eccentric loads.

© 2017 The Authors. Published by Elsevier Ltd. This is an open access article under the CC BY license (<http://creativecommons.org/licenses/by/4.0/>).

## 1. Introduction

During the past several decades, box girders have been widely applied in buildings and bridges due to their large bending and torsional stiffness. However, they are generally susceptible to the cross-sectional distortion [1] under eccentric loads due to their quadrilateral instability. Therefore, excessive distortional warping and transversal bending stresses will be produced besides the torsional and bending ones in box girders. In a special case, the distortional warping stresses may be significant to the torsional and bending ones. In order to control the distortion, diaphragms are installed at the interior of the girder, which can increase not only the stability of the local plate, but also the resistance to the warping deformations and stresses [2–4].

Researches on the distortion of girders with inner diaphragms have been performed for many decades. The distortion of box girder was initially studied by Dabrowski [5] who first formulated the distortion of box girders with a symmetrical cross section. Li [6,7] proposed that the shear strain of the cross section cannot be ignored when the distortional shear rigidity is significant compared to the distortional warping one for box girders. Wright [8] proposed the Beam on Elastic Foundation (BEF) analogy for the distortion of girders with inner diaphragms, where the diaphragms are analogous to inner supports. Based on BEF, Hsu [9,10] proposed the Equivalent Beam on Elastic Foundation (EBEF) analogy considering the shear strain of the cross section, and found that the EBEF analogy is more versatile than BEF due to its simplicity in analyzing more complex problems such as non-uniform sections and multi-span beams.

Interactions between the girder and diaphragms is the key issue for the distortion of girders with inner diaphragms. A statically indeterminate structure [11] was modeled with redundant forces acting along the junctions between the girder and diaphragms.

\* Corresponding author at: Key Lab of Civil Engineering Safety and Durability of China Education Ministry, Department of Civil Engineering, Tsinghua University, Beijing 100084, China.

E-mail address: [renyz66@mail.tsinghua.edu.cn](mailto:renyz66@mail.tsinghua.edu.cn) (Y. Ren).

Moreover, the force method was applied to calculate redundant forces, where elements in the stiffness matrix were obtained from the finite strip method [12]. The numerical results were then extended to multi-span bridges [13] and long-span curved bridges [14]. An outstanding contribution was made by Suetake [15], where the girder was regarded as an assembly of thin plates, and the extended trigonometric series method (ETS) was applied to analyze the stresses and deformations for box girders. Comparisons with FEM results show that ETS has a high accuracy. However, it is inconvenient to apply since there are many simultaneous nonlinear equations to solve even for girders with few diaphragms, e.g. there are up to 720 equations for a girder with two diaphragms.

The wall thickness of diaphragms and the number of diaphragms in a girder will make a significant influence on the displacements and stresses. Park [16,17] proposed a new beam element with nine degrees of freedom per node for girders. Studies showed that the distortional warping and transversal bending stresses were reduced by increasing the diaphragm number. Similar conclusions can be drawn for straight multi-cell box girders with diaphragms [18,19]. For horizontally curved bridges, the rational spacing between adjacent diaphragms was provided [20] according to the ratio between the distortional warping stress and the bending stress. Using FEM, Zhang [21] found that the rational number for diaphragms is 3 to 5 when the ratio of width to height of the cross section is 1.5 and the rational number is 9 when the ratio is 4.5. Li [22] proposed a new finite element solution, and found that the distortional warping stress for cantilever girders can be ignored when the spacing between adjacent diaphragms is less than one fifth of the span; while for simply supported and fixed girders, the spacing is less than one eighth of the span.

Initial parameter method (IPM) was proposed first by Vlasov [23] to analyze the non-uniform torsion of beams. Analogous to IPM in non-uniform torsion, IPM can be extended to analyze distortions of girders. Considering the effect of shear strains of the cross section, Xu [24,25] developed an equation with the variable distortional angle, and established two categories of IPMs of the fourth order, classified by the ratio of the distortional stiffness. Harashima [26] proposed a distortional equation with a distortional warping function, and established the fifth-order IPM. Both IPMs in distortion have a high efficiency compared with FEM. However, IPMs has not been extended into the distortion for girders with inner diaphragms.

For distortions of a girder with inner diaphragms, an assumption of infinite-rigidity diaphragm was generally made in most studies [16,20,27], where the in-plane deformation of diaphragms was totally restrained and warping was free. Similar assumptions can be found in distortion of curved box beams [28], where the distortional angle at the location of diaphragms is set as zero. However, the infinite-rigidity assumption is just an approximation, which is not applicable to thin flexible diaphragms. The main objective of this work is to investigate the distortion of simply supported girders with inner flexible diaphragms under concentrated eccentric loads, where the in-plane shear deformation of diaphragms is fully considered. Interactions between the girder and diaphragms are indicated by a distortional moment. Based on the compatibility condition between the girder and diaphragms, solutions for both the distortional angle and warping function are obtained from the IPM. Taking a simply supported girder with 2, 5 and 9 diaphragms, respectively, as an example, the distortional solutions from IPM were obtained, then verified by a FE analysis and experiments. This was followed by a parametric study, in which distortional deformations and stresses were investigated in terms of the diaphragm number and thickness and the height to span ratio of the girder. Based on the proposed IPM, stabilities of both the local web plate and mid-span diaphragm were examined for girders with three symmetrical inner diaphragms. A series of curves were obtained for the relations between the critical buckling load and the position of diaphragms under various height to width ratios of the cross section.

### 2. Structural model

Consider a simply supported box girder with inner diaphragms under concentrated eccentric loads  $P_j$  ( $j = 1, 2, \dots, m$ ). The coordinate system  $O$ - $xyz$  is illustrated in Fig. 1a with the original  $O$  at the shear center on one end of the girder. For analysis, the distances between  $O$  and the mid-lines of webs B and D are marked by  $n_1$  and  $n_2$  in Fig. 1b, respectively. The girder is made of a homogeneous, isotropic and linearly elastic material with its Young's and shear moduli denoted by  $E$  and  $G$ , respectively. The girder span is  $l$ . The thicknesses of web B and D are  $t_1$  and  $t_2$  and their height is  $h$ , while the width of flanges A and C is  $b$  and the thickness  $t_3$ . The thickness for the  $i$ th diaphragm is  $t_{pi}$  ( $i = 1, 2, \dots, n$ ) and its mid line is marked by  $z_{pi}$ , measured from  $O$ . The load  $P_j$  is located on the top of web D at  $z_j$ .

Fig. 2a shows that the eccentric load  $P_j$  can be decomposed into three components [29,30] – the flexural load, the torsional and the

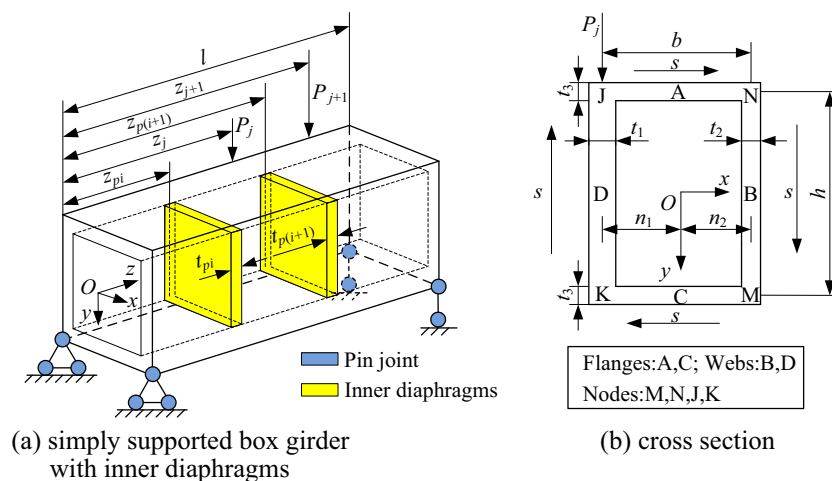


Fig. 1. Girder with inner diaphragms under eccentric loads  $P_j$  ( $j = 1, 2, \dots, m$ ).

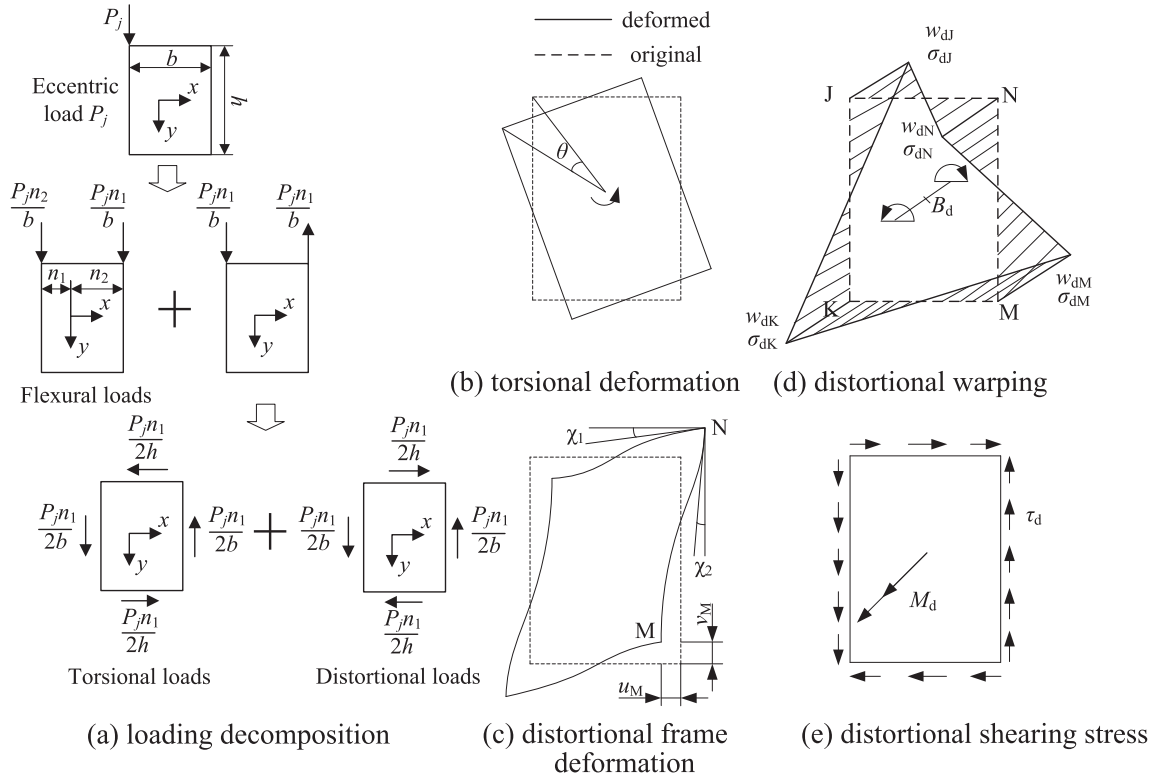


Fig. 2. Loading decomposition, deformations and stresses of girders.

distortional load. In Fig. 2b, the cross-section rigidly rotates around  $O$  with a torsional angle  $\theta$  under torsional loads. Fig. 2c illustrates the transversal deformations in the web and the flange under distortional loads, where  $u_M$  and  $v_M$  are horizontal and vertical displacements at node  $M$ , respectively. The variation of the right angle at node  $N$  is defined as the distortional angle  $\chi$ , given by  $\chi = \chi_1 + \chi_2$ . Moreover, the warping displacement  $w_d$  and the stress  $\sigma_d$ , produced by the distortional moment  $B_d$ , are shown in Fig. 2d. There also exists the shear stress  $\tau_d$  along the cross-section profile, developed by the distortional moment  $M_d$ , as shown in Fig. 2e.

This article will focus on the distortional deformation and stresses of a simply supported box girder with inner diaphragms subjected to concentrated eccentric loads.

### 3. Distortion of girders without diaphragm

In distortion, when the shear stiffness of the cross section has a significant value in comparison with the warping one, the influence of shear strain of the cross section on deformation and stresses cannot be ignored [6,7]. The distortional differential equation can be expressed as [7]

$$EI_t W(z)'''' - EI_c \frac{EI_t}{GI_k} W(z)'' + EI_c W(z) = m_d' \quad (1)$$

where  $I_t$ ,  $I_c$  and  $I_k$  are distortional warping, frame and shear constants, respectively;  $W(z)$  is the distortional warping function;  $m_d$  is the distributed distortional moment. The number of the apostrophes of  $W(z)$  indicates the first, second and fourth differentiations with respect to the  $z$ -coordinate.

Under concentrated distortional loads,  $m_d = 0$ , and the solution for Eq. (1) is given as [26]

$$W(z) = \sum_{i=1}^4 B_i \varphi_i(z) \quad (2)$$

where  $B_i$  ( $i = 1, 2, 3, 4$ ) are coefficients determined by the boundary conditions, and  $\varphi_i$  are defined as  $\varphi_1 = \cosh(\lambda_1 z) \sin(\lambda_2 z)$ ,  $\varphi_2 = \cosh(\lambda_1 z) \cos(\lambda_2 z)$ ,  $\varphi_3 = \sinh(\lambda_1 z) \cos(\lambda_2 z)$ ,  $\varphi_4 = \sinh(\lambda_1 z) \sin(\lambda_2 z)$  where  $\lambda_i$  ( $i = 1, 2$ ) are distortional coefficients.

$$\lambda_1 = \frac{1}{2} \sqrt{\sqrt{\frac{4EI_c}{EI_t} + \frac{EI_c}{GI_k}}}, \lambda_2 = \frac{1}{2} \sqrt{\sqrt{\frac{4EI_c}{EI_t} - \frac{EI_c}{GI_k}}}$$

Relations between the warping function and the distortional angle are [7]

$$\chi(z) = -\frac{EI_t}{EI_c} W'''(z), B_d(z) = -EI_t W'(z) M_d(z) = -EI_t W''(z) \quad (3)$$

Substituting Eq. (2) into Eq. (3), the matrix equation is given by  $\mathbf{Z}(z) = \Phi(z)\mathbf{B}$  (4)

where

$$\Phi(z) = \begin{bmatrix} -\frac{EI_t}{EI_c} \varphi_1'''(z) & -\frac{EI_t}{EI_c} \varphi_2'''(z) & -\frac{EI_t}{EI_c} \varphi_3'''(z) & -\frac{EI_t}{EI_c} \varphi_4'''(z) \\ \varphi_1(z) & \varphi_2(z) & \varphi_3(z) & \varphi_4(z) \\ \varphi_1'(z) & \varphi_2'(z) & \varphi_3'(z) & \varphi_4'(z) \\ \varphi_1''(z) & \varphi_2''(z) & \varphi_3''(z) & \varphi_4''(z) \end{bmatrix}, \mathbf{B} = B_1, B_2, B_3, B_4^T \quad (5)$$

$\mathbf{Z}(z)$  is the state vector in IPM,

$$\mathbf{Z}(z) = \left\{ \chi(z), W(z), -\frac{B_d(z)}{EI_t}, \frac{M_d(z)}{EI_t} \right\}^T \quad (6)$$

The boundary conditions for a simply supported girder are

$$\chi(0) = 0, B_d(0) = 0, \quad \text{for the initial end } z = 0;$$

$$\chi(l) = 0, B_d(l) = 0, \quad \text{for the ultimate end } z = l.$$

Correspondingly, the state vectors on both ends are

$$\begin{aligned} \mathbf{Z}(0) &= \left\{ 0, \quad W(0), \quad 0, \quad \frac{M_d(0)}{EI_t} \right\}^T, \quad \mathbf{Z}(l) \\ &= \left\{ 0, \quad W(l), \quad 0, \quad \frac{M_d(l)}{EI_t} \right\}^T \end{aligned}$$

For  $z = 0$ ,  $\mathbf{Z}(0) = \Phi(0)\mathbf{B}$ , we have

$$\mathbf{B} = [\Phi(0)]_{\text{inv}} \cdot \mathbf{Z}(0) \tag{7}$$

where  $[\Phi(0)]_{\text{inv}}$  is the inverse matrix of  $\Phi(0)$ .

Substituting Eq. (7) into Eq. (4) yields in the state vector  $\mathbf{Z}(z)$

$$\mathbf{Z}(z) = \mathbf{P}(z) \cdot \mathbf{Z}(0) \tag{8}$$

where  $\mathbf{P}(z)$  is the transfer matrix, and  $\mathbf{P}(z) = \Phi(z) \cdot [\Phi(0)]_{\text{inv}}$ .

Eq. (8) is the standard form of IPM for the distortion of girders without diaphragms. However, the transfer matrix  $\mathbf{P}(z)$  is complicated. Based on the relations between  $\varphi_i(z)$  ( $i = 1, 2, 3, 4$ ) and their differentiations (see Eq. (A1)–(A3) in Appendix A), the matrix  $\mathbf{P}(z)$  is simplified as

$$\mathbf{P}(z) = \begin{bmatrix} -SC_1'''(z) & -KC_2'''(z) & -SKC_3'''(z) & KC_4'''(z) \\ \frac{S}{K}C_1(z) & C_2(z) & SC_3(z) & -C_4(z) \\ \frac{S}{K}C_1'(z) & C_2'(z) & SC_3'(z) & -C_4'(z) \\ -\frac{S}{K}C_1''(z) & -C_2''(z) & -SC_3''(z) & C_4''(z) \end{bmatrix} \tag{9}$$

where  $S = \frac{1}{2i_1^2 + 2i_2^2}$ ,  $K = \frac{EI_t}{EI_c}$ ,  $C_1(z) = \frac{\varphi_3(z)}{\lambda_1} - \frac{\varphi_1(z)}{\lambda_2}$ ,  $C_2(z) = \varphi_2(z) - \frac{\lambda_1^2 - \lambda_2^2}{2\lambda_1\lambda_2} \varphi_4(z)$ ,  $C_3(z) = \frac{3\lambda_1^2 - \lambda_2^2}{\lambda_1} \varphi_3(z) - \frac{\lambda_1^2 - 3\lambda_2^2}{2\lambda_1\lambda_2} \varphi_1(z)$ ,  $C_4(z) = \frac{\varphi_4(z)}{2\lambda_1\lambda_2}$ .

The  $j$ th distortional load in IPM is indicated by a vector  $\mathbf{Z}_j$ , given by

$$\mathbf{Z}_j = \left\{ 0, \quad 0, \quad 0, \quad \frac{M_j}{EI_t} \right\}^T \tag{10}$$

where  $M_j$  is the distortional moment for the  $j$ th distortional load, and  $M_j = P_j n_1/2$  [26];  $n_1$  is the distance between the web D and point the original  $O$  (see Fig. 1b).

### 4. Distortion of box girders with inner diaphragms

#### 4.1. IPM solution

For analysis, a statically indeterminate structure is modeled with inner redundant forces acting along the junctions between the girder and the diaphragms. The entire model is shown in Fig. 3a and the horizontal and vertical redundant forces  $H_{ej}$  and  $V_{ej}$  are illustrated in the zoomed picture, where the subscript  $e$  indicates the webs and flanges and  $e = A, B, C, D$  (see Fig. 1b). The

small circles indicate the joints between the girder and diaphragms where redundant forces are located.

In order to analyze the interactions between the girder and diaphragms, two assumptions are made:

- (1) Self balance of the in-plane forces of diaphragms

Under distortional loads, the summation of all vertical and horizontal redundant forces and moments are zero for diaphragms. That is

$$\sum_{e=A,B,C,D} \sum_{j=2}^r H_{ej} = 0, \quad \sum_{e=A,B,C,D} \sum_{j=2}^r V_{ej} = 0, \quad \sum_{e=A,B,C,D} \sum_{j=2}^r H_{ej} y_{ej} + \sum_{e=A,B,C,D} \sum_{j=2}^r V_{ej} x_{ej} = 0 \tag{11}$$

where  $x_{ej}$  and  $y_{ej}$  are the distances between the redundant forces  $V_{ej}$ ,  $H_{ej}$  and the original  $O$ .

Based on the self balance assumption, only the distortional component for redundant forces is reserved. Referred to the formation of external moment  $M_j$  [26,27], the distortional components of the redundant forces are gathered and indicated by a concentrated distortional moment  $M_{pi}$  for the  $i$ th diaphragm. Therefore, the interactions between the girder and diaphragms can be indicated by a moment  $M_{pi}$  ( $i = 1, 2, \dots, n$ ). Only  $M_{pi}$ , opposite to  $M_j$ , will resist the distortional deformation and stresses. In IPM,  $M_{pi}$  is indicated by a vector  $\mathbf{Z}_{pi}$ , given by

$$\mathbf{Z}_{pi} = \left\{ 0, \quad 0, \quad 0, \quad \frac{M_{pi}}{EI_t t_{pi}} \right\}^T \tag{12}$$

- (2) Compatibility condition between the girder and diaphragms

In-plane shear strains of diaphragms are considered, given by  $\gamma_{pi} = M_{pi} / (Gbh_{pi})$ . The compatibility condition is that the distortional angle at the mid line of diaphragms is opposite to the in-plane shear strain of diaphragms. That is  $\chi(z_{pi}) = -\gamma_{pi}$  ( $0 \leq i \leq n$ ). This is a key aspect for the distortion of girders with inner diaphragms.

Combining Eq. (8) and Eq. (12), the state vector  $\mathbf{Z}(z)$  can be expressed as

$$\mathbf{Z}(z) = \mathbf{P}(z)\mathbf{Z}(0) - \sum_{i=1}^R \int_{z_{pi}-t_{pi}/2}^{z_{pi}+t_{pi}/2} \mathbf{P}(z-z_i)\mathbf{Z}_{pi} dz_i - \sum_{j=1}^S \mathbf{P}(z-z_j)\mathbf{Z}_j \tag{13}$$

where  $R$  and  $S$  are the numbers of diaphragms and moments  $M_j$  before point  $z$ , respectively. The transfer matrices  $\mathbf{P}(z-z_i)$  and  $\mathbf{P}$

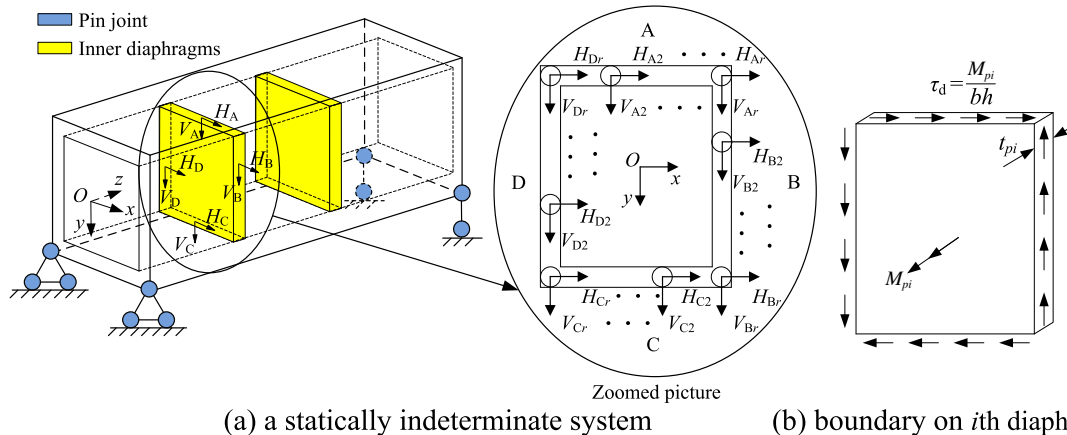


Fig. 3. A statically indeterminate structure and the equivalent boundaries for the  $i$ th diaphragm.

$(z - z_j)$  are obtained from  $\mathbf{P}(z)$  by substituting the variable  $z$  by ' $z - z_i$ ' and ' $z - z_j$ '.

For  $z = l$ , Eq. (13) changes into

$$\mathbf{Z}(l) = \mathbf{P}(l)\mathbf{Z}(0) - \sum_{i=1}^n \int_{z_{pi}-t_{pi}/2}^{z_{pi}+t_{pi}/2} \mathbf{P}(l-z_i)\mathbf{Z}_{pi}dz_i - \sum_{j=1}^m \mathbf{P}(l-z_j)\mathbf{Z}_j \quad (14)$$

where the vectors  $\mathbf{Z}(l)$  and  $\mathbf{Z}(0)$  are referred to Eq. (6);  $W(0)$  and  $M_d(0)$  in vector  $\mathbf{Z}(0)$  can be calculated from the first and third simultaneous equations in Eq. (14). Then, substituting  $W(0)$  and  $M_d(0)$  into Eq. (13), the distortional angle and the warping function can be obtained as

$$\chi(z) = \frac{\sum_{i=1}^n {}^1\eta_i(z)M_{pi} + \sum_{j=1}^m {}^1\epsilon_{24}(z, z_j)M_j}{2\lambda_1\lambda_2EI_c\Phi_{24}(l, l)} \quad (15)$$

$$W(z) = \frac{\sum_{i=1}^n {}^2\eta_i(z)M_{pi} + \sum_{j=1}^m {}^2\epsilon_{24}(z, z_j)M_j}{2\lambda_1\lambda_2EI_t\Phi_{24}(l, l)} \quad (16)$$

where

$${}^R_1\eta_i(z) = \frac{2}{t_{pi}} \left[ \zeta_{31}^{00} \left( l - z_{pi}, \frac{t_{pi}}{2} \right) \Phi_{42}^{33}(z, l) + \zeta_{31}^{02} \left( l - z_{pi}, \frac{t_{pi}}{2} \right) \Phi_{42}^{13}(l, z) \right] - H \left( R + \frac{1}{2} - i \right) \frac{2\Phi_{24}(l, l)}{t_{pi}} \zeta_{31}^{02} \left( z - z_{pi}, \frac{t_{pi}}{2} \right)$$

$${}^R_2\eta_i(z) = \frac{2}{t_{pi}} \left[ \zeta_{31}^{00} \left( l - z_{pi}, \frac{t_{pi}}{2} \right) \Phi_{42}^{30}(l, z) - \zeta_{31}^{02} \left( l - z_{pi}, \frac{t_{pi}}{2} \right) \Phi_{42}^{10}(l, z) \right] + H \left( R + \frac{1}{2} - i \right) \frac{2\Phi_{24}(l, l)}{t_{pi}} \zeta_{31}^{0(-1)} \left( z - z_{pi}, \frac{t_{pi}}{2} \right)$$

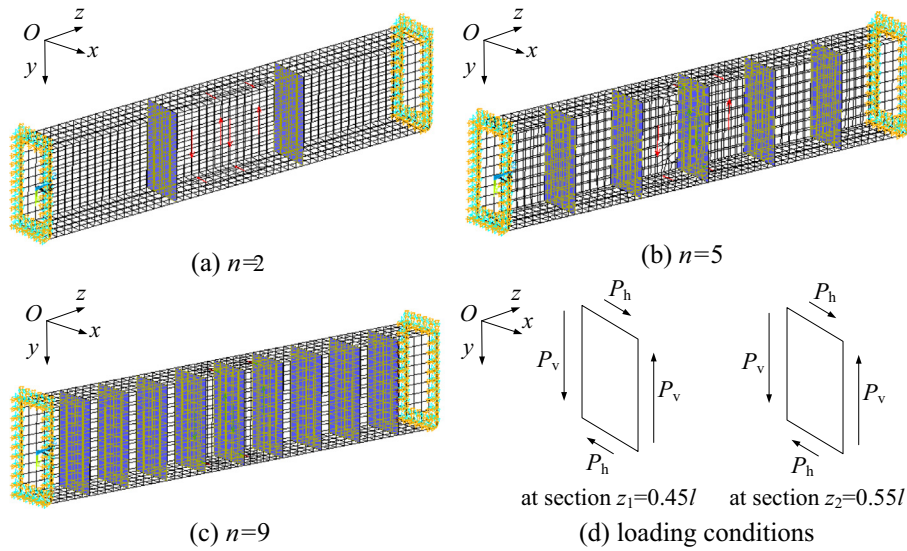


Fig. 4. Meshing grid, ending boundaries and loading conditions in FEA model.

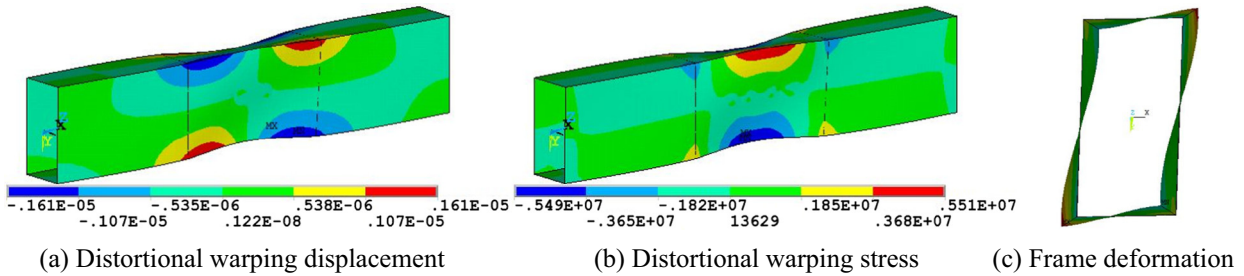


Fig. 5. 3D contours of a girder with two diaphragms under distortional loads ( $t_p = 0.01$  m, amp = 3000).

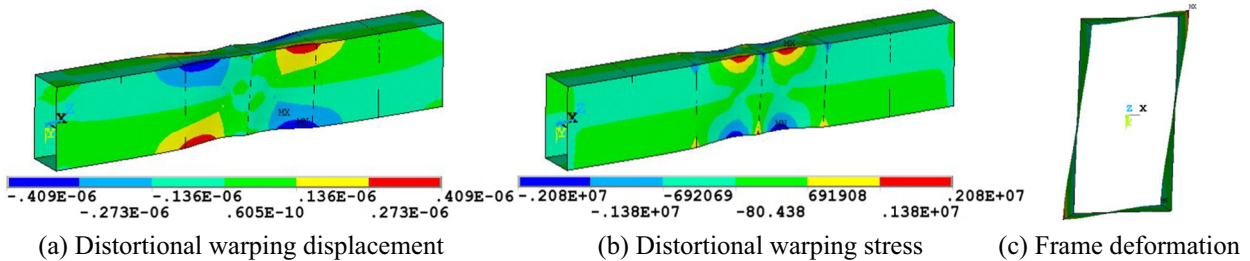


Fig. 6. 3D contours of a girder with five diaphragms under distortional loads ( $t_p = 0.01$  m, amp = 10,000).

$$s^1 \varepsilon_{24}(z, z_j) = \Lambda_{24}(z, z_j) - H\left(S + \frac{1}{2} - j\right) \varphi_4'''(z - z_j) \Phi_{24}(l, l)$$

$$s^2 \varepsilon_{24}(z, z_j) = \overline{\Lambda}_{24}(z, z_j) + H\left(S + \frac{1}{2} - j\right) \varphi_4(z - z_j) \Phi_{24}(l, l)$$

$H(x)$  is the unit step function.  $H(x) = 1$  for  $x > 0$  and  $H(x) = 0$  for  $x < 0$

$$\Phi_{ij}(x, y) = \begin{vmatrix} \varphi_i'''(x) & \varphi_j'''(y) \\ \varphi_i'(x) & \varphi_j'(y) \end{vmatrix}, \quad \overline{\Lambda}_{ij}(x, y) = \begin{vmatrix} \varphi_i(x) & \Phi_{4i}(l - y, l) \\ \varphi_j(x) & \Phi_{4j}(l - y, l) \end{vmatrix},$$

$$\Lambda_{ij}(x, y) = \frac{d^3 \overline{\Lambda}_{ij}(x, y)}{dx^3}$$

$$\Phi_{mn}^{ij}(x, y) = \begin{vmatrix} \varphi_m^{(i)}(x) & \varphi_n^{(i)}(x) \\ \varphi_m^{(j)}(y) & \varphi_n^{(j)}(y) \end{vmatrix}, \quad \xi_{mn}^{ij}(x, y) = \begin{vmatrix} \varphi_m^{(i)}(x) & -\varphi_n^{(i)}(x) \\ \varphi_m^{(j)}(y) & \varphi_n^{(j)}(y) \end{vmatrix}$$

where  $\varphi_m^{(i)}(x)$  and  $\varphi_n^{(i)}(y)$  are the  $i$ th differentiation of functions  $\varphi_m(x)$  and  $\varphi_n(y)$ .  $\varphi_n^{(-1)}(y)$  is the integral of function  $\varphi_n(y)$ , given by

$$\varphi_2^{(-1)}(y) = \frac{\lambda_1 \varphi_3(y) + \lambda_2 \varphi_1(y)}{\lambda_1^2 + \lambda_2^2}, \quad \varphi_4^{(-1)}(y) = \frac{\lambda_1 \varphi_1(y) - \lambda_2 \varphi_3(y)}{\lambda_1^2 + \lambda_2^2}$$

When the calculated point  $z$  is located in the thickness of  $(R + 1)$  th diaphragm ( $z_{p(R+1)} - t_{p(R+1)}/2 \leq z \leq z_{p(R+1)} + t_{p(R+1)}/2$ ), an additional angle  $\chi_{add}$  and function  $W_{add}$  should be involved,

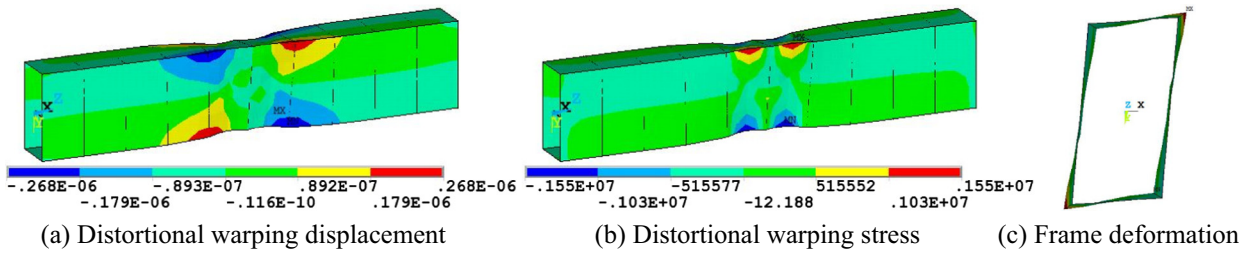


Fig. 7. 3D contours of a girder with nine diaphragms under distortional loads ( $t_p = 0.01$  m, amp = 20,000).

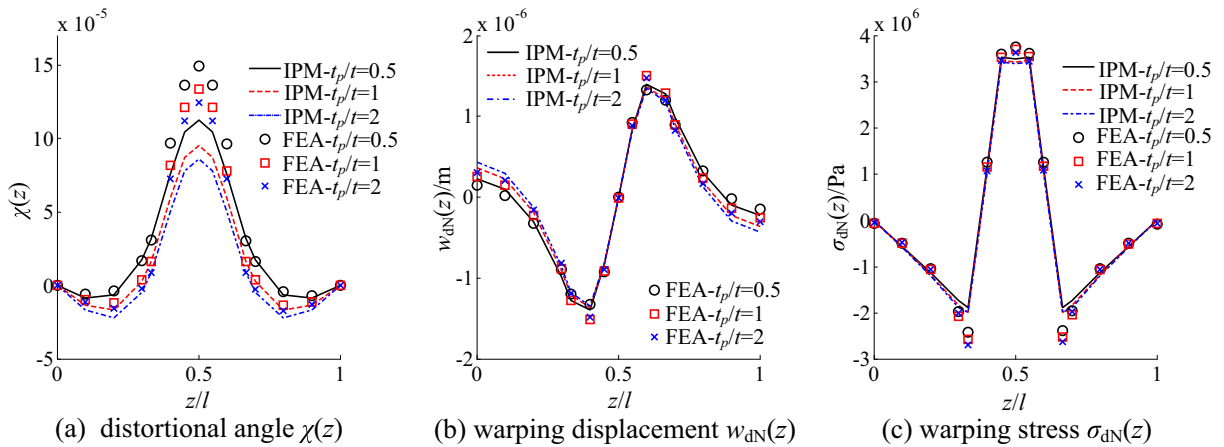


Fig. 8. The distortional angle, warping displacements and stresses between IPM and FEA for a simply supported girder with two diaphragms of different diaphragm thicknesses.

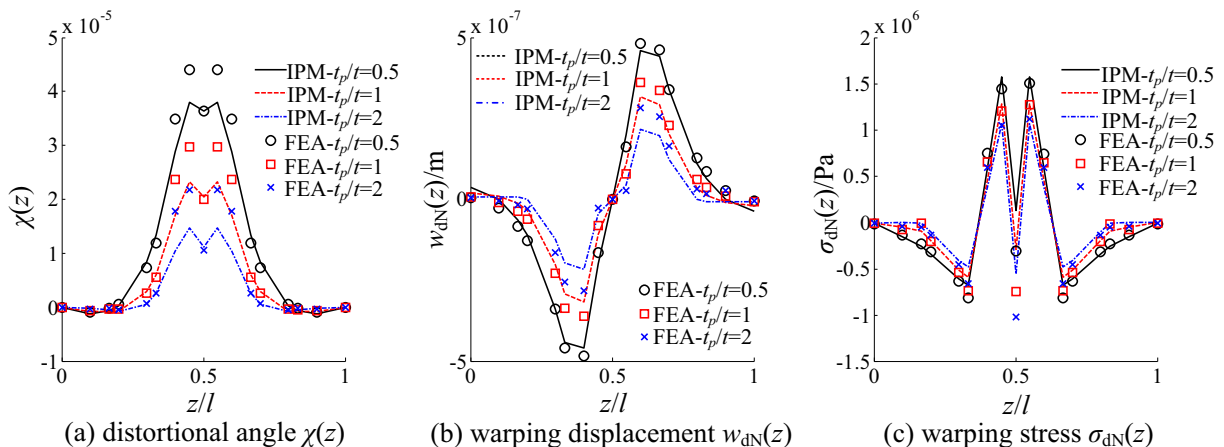


Fig. 9. The distortional angle, warping displacements and stresses between IPM and FEA for simply supported girders with five diaphragms varying with three diaphragm thicknesses.

$$\chi_{\text{add}} = \frac{M_{p(R+1)}[2\lambda_1\lambda_2 - \varphi_4''(z - z_{p(R+1)} + t_{p(R+1)}/2)]}{2\lambda_1\lambda_2 EI_t t_{p(R+1)}} \quad (17)$$

$$W_{\text{add}} = \frac{M_{p(R+1)}\varphi_4^{(-1)}(z - z_{p(R+1)} + t_{p(R+1)}/2)}{2\lambda_1\lambda_2 EI_t t_{p(R+1)}} \quad (18)$$

where  $z_{p(R+1)}$ ,  $t_{p(R+1)}$  and  $M_{p(R+1)}$  are the mid-line location, the thickness and the distortional moment of the  $(R + 1)$ th diaphragm, respectively.

Based on Eqs. (15)–(18), both the angle  $\chi(z)$  and the function  $W(z)$  are related to  $M_j$  and  $M_{pi}$ . Since  $M_j$  has been given in Eq. (10), solutions rest in  $M_{pi}$ .

#### 4.2. Derivation of $M_{pi}$

The compatibility condition gives the equation

$$\sum_{i=1}^n T^1 \eta_i(z_{pT}) M_{pi} + \sum_{j=1}^m T^1 \varepsilon_{24}(z_{pT}, z_j) M_j - \frac{\Phi_{24}(l, l)}{t_{pT}} \left[ \varphi_4''\left(\frac{t_{pT}}{2}\right) - 2\lambda_1\lambda_2 \left(1 + \frac{EI_c}{Gbh}\right) \right] M_{pT} = 0 \quad (19)$$

for the  $T$ th diaphragm ( $T = 1, 2, \dots, n$ ), where

$$T^1 \eta_i(z_{pT}) = \frac{2}{t_{pi}} \left[ \xi_{31}^{00} \left( l - z_{pi}, \frac{t_{pi}}{2} \right) \Phi_{42}^{33}(z_{pT}, l) + \xi_{31}^{02} \left( l - z_{pi}, \frac{t_{pi}}{2} \right) \Phi_{42}^{13}(l, z_{pT}) \right] - H\left(T - \frac{1}{2} - i\right) \frac{2\Phi_{24}(l, l)}{t_{pi}} \xi_{31}^{02} \left( z_{pT} - z_{pi}, \frac{t_{pi}}{2} \right)$$

$$T^1 \varepsilon_{24}(z_{pT}, z_j) = \Lambda_{24}(z_{pT}, z_j) - H\left(k_T + \frac{1}{2} - j\right) \Phi_{24}(l, l) \varphi_4''(z_{pT} - z_j)$$

$k_T$  is the number of distortional loads before the  $T$ th diaphragm.

The matrix equation system for Eq. (19) is

$$\boldsymbol{\eta} \cdot \mathbf{M}_p + \boldsymbol{\varepsilon} = \mathbf{0} \quad (20)$$

where

$$\mathbf{M}_p = \{M_{p1}, M_{p2}, \dots, M_{pn}\}^T; \quad \boldsymbol{\eta} = \begin{bmatrix} R_{11} & T^1 \eta_2(z_{p1}) & T^1 \eta_n(z_{p1}) \\ T^1 \eta_1(z_{p2}) & R_{22} & T^1 \eta_n(z_{p2}) \\ \dots & \dots & \dots \\ T^1 \eta_1(z_{pn}) & T^1 \eta_2(z_{pn}) & R_{nn} \end{bmatrix}$$

$$\boldsymbol{\varepsilon} = \left[ \sum_{j=1}^m T^1 \varepsilon_{24}(z_{p1}, z_j) M_j, \sum_{j=1}^m T^1 \varepsilon_{24}(z_{p2}, z_j) M_j, \dots, \sum_{j=1}^m T^1 \varepsilon_{24}(z_{pn}, z_j) M_j \right]^T$$

and the diagonal elements in matrix  $\boldsymbol{\eta}$  is

$$R_{ii} = T^1 \eta_i(z_{pi}) - \frac{\Phi_{24}(l, l)}{t_{pi}} \left[ \varphi_4''\left(\frac{t_{pi}}{2}\right) - 2\lambda_1\lambda_2 \left(1 + \frac{EI_c}{Gbh}\right) \right]$$

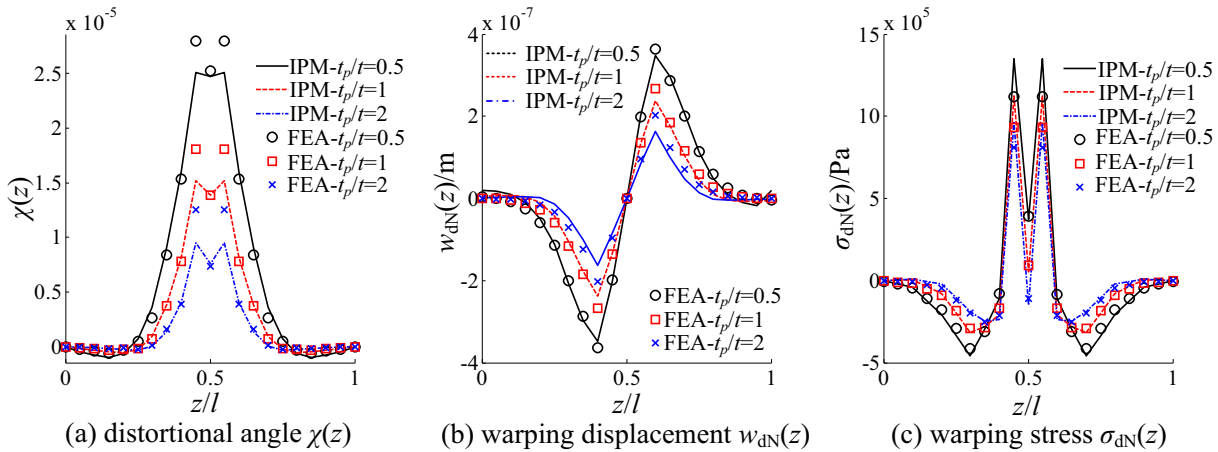


Fig. 10. The distortional angle, warping displacements and stresses between IPM and FEA for simply supported girders with nine diaphragms varying with three diaphragm thicknesses.

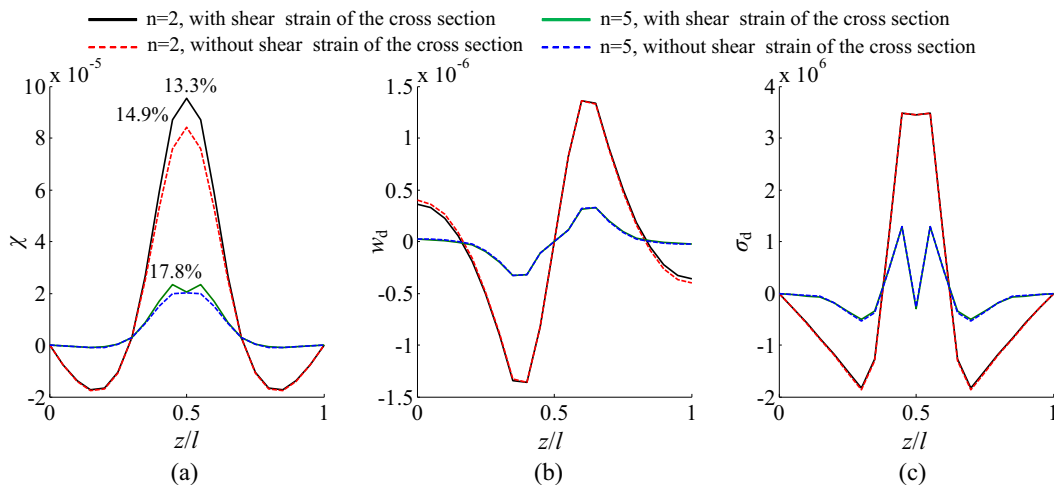


Fig. 11. Comparison of girders with and without the shear strain of cross section for (a) the distortional angle, (b) warping displacements and (c) stresses of simply supported girders with 2 and 5 diaphragms.

Consequently,  $M_{pi}$  can be obtained by

$$M_{pi} = -\sum_{j=1}^m Q_{ij}M_j \quad (21)$$

according to the Cramer rule,  $Q_{ij} = |\eta_i|/|\eta|$ , where the  $|\eta|$  indicates the determinant of  $\eta$ , and  $\eta_i$  is the same of  $\eta$  except for the  $i$ th column  $[T^1 \varepsilon_{24}(z_{p1}, z_j), T^1 \varepsilon_{24}(z_{p2}, z_j), \dots, T^1 \varepsilon_{24}(z_{pm}, z_j)]^T$

### 4.3. Simplification of $\chi(z)$ and $W(z)$

Substituting Eq. (21) into Eq. (15), and the angle  $\chi(z)$  changes into

$$\chi(z) = \frac{\sum_{i=1}^n \sum_{j=1}^m \left( \frac{s^1 \varepsilon_{24}(z, z_j)}{n} - R^1 \eta_i(z) Q_{ij} \right) M_j}{2\lambda_1 \lambda_2 E I_c \Phi_{24}(l, l)} \quad (22)$$

where  $n$  and  $m$  are the total numbers of diaphragms and distortional loads, respectively.

The number of calculation steps is  $m \times n$  in Eq. (22) and it would be time-consuming for girders with many diaphragms under many distortional loads. For solution, a matrix equation is established, given by

$$\eta \cdot \psi = \alpha \quad (23)$$

where  $\psi = \begin{pmatrix} \psi_{11} & \psi_{12} & \dots & \psi_{1n} \\ \psi_{21} & \psi_{22} & \dots & \psi_{2n} \\ \dots & \dots & \dots & \dots \\ \psi_{m1} & \psi_{m2} & \dots & \psi_{mn} \end{pmatrix}$ ;  $\alpha = \begin{pmatrix} \alpha_{11} & \alpha_{12} & \dots & \alpha_{1n} \\ \alpha_{21} & \alpha_{22} & \dots & \alpha_{2n} \\ \dots & \dots & \dots & \dots \\ \alpha_{m1} & \alpha_{m2} & \dots & \alpha_{mn} \end{pmatrix}$  and the elements in matrix  $\alpha$  are

$$\alpha_{gk} = \begin{cases} \sum_{j=1}^m [s^1 \varepsilon_{24}(z, z_j) T^1 \eta_k(z_{pg}) / n - R^1 \eta_g(z) T^1 \varepsilon_{24}(z_{pg}, z_j)] M_j & (g \neq k) \\ \sum_{j=1}^m [s^1 \varepsilon_{24}(z, z_j) R_{gg} / n - R^1 \eta_g(z) T^1 \varepsilon_{24}(z_{pg}, z_j)] M_j & (g = k) \end{cases}$$

In this approach, the distortional angle  $\chi(z)$  can be simplified as

$$\chi(z) = \frac{1}{2\lambda_1 \lambda_2 E I_c \Phi_{24}(l, l)} \sum_{i=1}^n \psi_{ii} \quad (24)$$

For the warping function  $W(z)$ , a matrix equation can also be established similar to Eq. (23), and the elements  $\alpha_{gk}$  ( $g, k = 1, 2, \dots, n$ ) in matrix  $\alpha$  are

$$\alpha_{gk} = \begin{cases} \sum_{j=1}^m [s^2 \varepsilon_{24}(z, z_j) T^1 \eta_k(z_{pg}) / n - R^2 \eta_g(z) T^1 \varepsilon_{24}(z_{pg}, z_j)] M_j & (g \neq k) \\ \sum_{j=1}^m [s^2 \varepsilon_{24}(z, z_j) R_{gg} / n - R^2 \eta_g(z) T^1 \varepsilon_{24}(z_{pg}, z_j)] M_j & (g = k) \end{cases}$$

Therefore, the function  $W(z)$  can be simplified as

$$W(z) = \frac{1}{2\lambda_1 \lambda_2 E I_t \Phi_{24}(l, l)} \sum_{i=1}^n \psi_{ii} \quad (25)$$

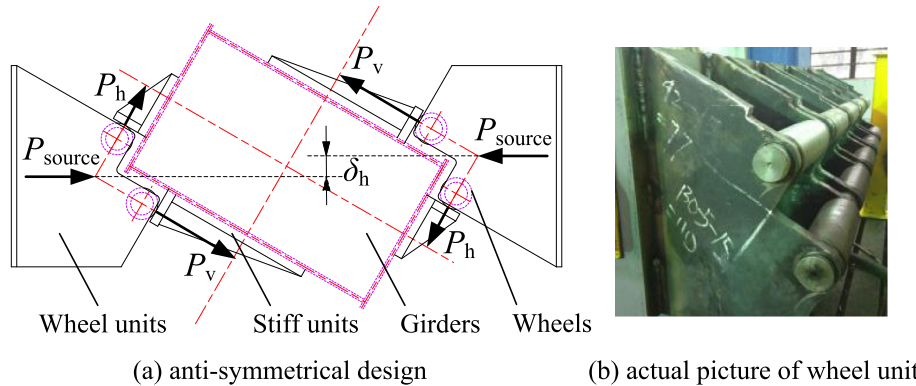


Fig. 12. anti-symmetrical loading design.

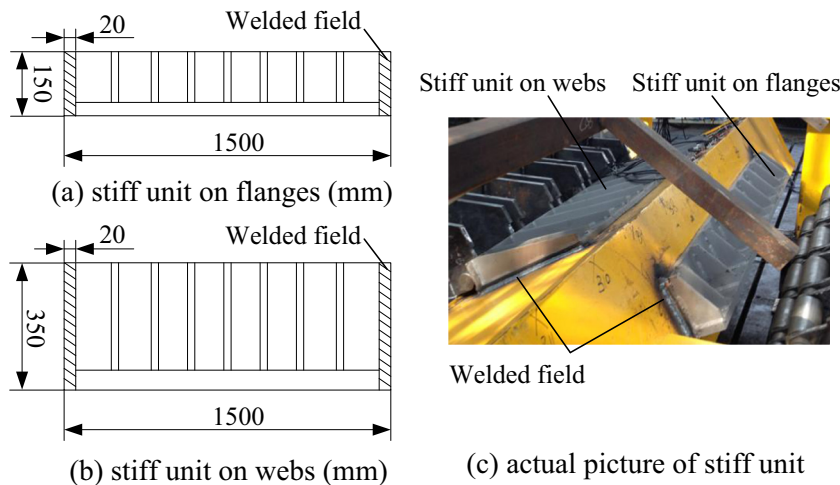


Fig. 13. Stiff units.

Taking the node N (see Fig. 1b) of the cross section as an example, the distortional warping displacement  $w_{dN}$  and the stress  $\sigma_{dN}$  are given by

$$w_{dN}(z) = -\frac{W(z)\beta_d bh}{4(\beta_d + 1)}, \sigma_{dN}(z) = -\frac{EW_I(z)\beta_d bh}{4(\beta_d + 1)} \quad (26)$$

where  $\beta_d$  is the ratio of the distortional warping stresses between nodes J and N, and  $\beta_d = \frac{3bt_3 + ht_1}{3bt_3 + ht_2}$

## 5. Verifications of IPM

### 5.1. Verifications with FEA

To verify the proposed IPM, simply supported girders with 2, 5 and 9 diaphragms are investigated for three diaphragm thicknesses, respectively by FEA using a commercial code ANSYS. All girders are modeled with the Young's modulus  $E = 2.1 \times 10^{11}$  Pa, the Poisson's ratio  $\nu = 0.3$ , the span  $l = 1$  m, the width  $b = 0.1$  m, the height  $h = 0.2$  m and the flanges and webs thicknesses  $t = 0.01$  m. Diaphragms are evenly distanced along the span with the thicknesses  $t_p = 0.005$  m, 0.01 m and 0.02 m, respectively.

Fig. 4a, b and c show the meshing grids of the girders and diaphragms using Shell63 element in FEA model, where translations in the  $x$ - and  $y$ - axial directions and rotations about the  $y$ - and  $z$ -axes on both ends are restrained. A convergent test shows that 1650 to 2026 elements are adequate in terms of the diaphragm number. Fig. 4d shows the loading conditions, where two concentrated distortional loads are applied along the flange and web in

cross sections  $z_1 = 0.45l$  and  $z_2 = 0.55l$ , and  $P_h = 1.25$  kN and  $P_v = 2.5$  kN, respectively.

Figs. 5–7 show 3D contours of the distortional warping deformations and stresses for simply supported girders with 2, 5 and 9 diaphragms, respectively. The 'amp' indicates the amplified factor for deformations. It is seen that the largest displacement and stress occur at the junction between webs and flanges at the loading sections. With the increment of diaphragm number, the largest stress reduces from 5.51 MPa to 1.55 MPa and the displacement from 1.61  $\mu\text{m}$  to 0.268  $\mu\text{m}$ , and frame deformations at the loading sections clearly become small.

Figs. 8–10 show the distortional angle, warping displacements and stresses at node N from IPM and FEA for simply supported girders with 2, 5 and 9 diaphragms, respectively, in the relative diaphragm thickness  $t_p/t = 0.5, 1$  and 2. The distortional angle in FEA results can be calculated by Fig. 9

$$\chi(z) = \frac{UX_N - UX_M}{h} + \frac{UY_N - UY_J}{b} \quad (27)$$

where  $UX_N$  and  $UX_M$  are  $x$ -axial displacements at nodes N and M (see Fig. 1b), respectively;  $UY_J$  and  $UY_N$  are  $y$ -axial displacements at nodes J and N, respectively.

Good agreements are observed between IPM and FEA in Figs. 8–10 for the distortional angle, warping displacements and stresses for simply supported girders with inner diaphragms. Compared the girders braced by 2 diaphragms with those by 5 and 9 diaphragms, it's worth noting that the mid-span diaphragm effectively restrains the transversal deformation.

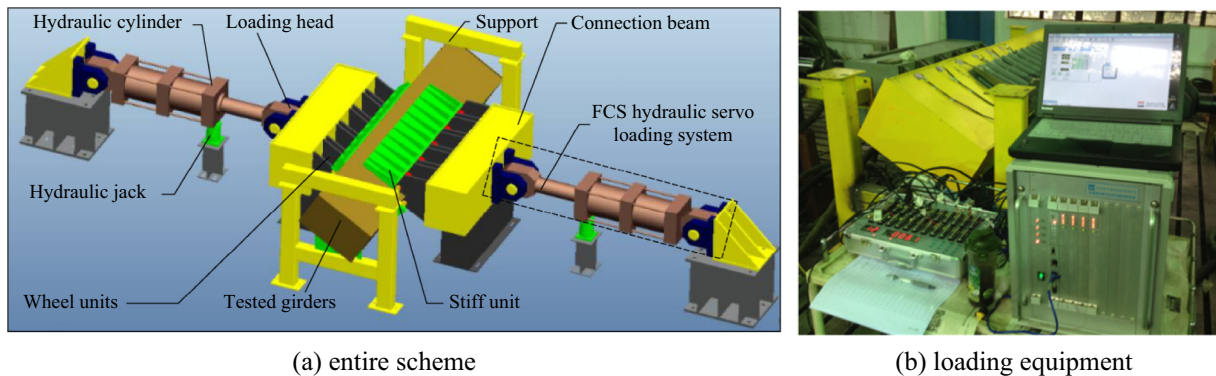


Fig. 14. Entire experimental scheme.

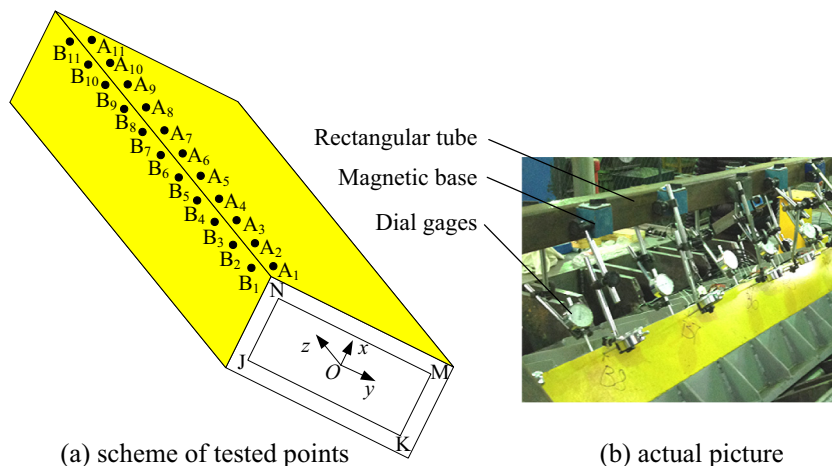


Fig. 15. The scheme of tested points.

For the distortional angle, the largest error between IPM and FEA occurs at the loading sections, where the FEA result is 23.68% higher than the IPM one for girders with two diaphragms, and reduces to 13.86% for those with five diaphragms and 10.18% for those with nine diaphragms. Since there is no diaphragms or stiffeners at the loading sections, the error between IPM and FEA can be attributed to the local stress concentration. So the distortional angle obtained from IPM is susceptible to the influence of stress concentration.

In addition, the influence of shear strains of the cross section on distortional deformations and stresses are examined in Fig. 11 for simply supported girders with 2 and 5 diaphragms, where the compatibility condition between the girder and diaphragms is considered. It is seen that the shear strain of the cross section makes little effect on warping displacements and stresses, but a large influence on the distortional angle. The largest difference occurs at the loading sections  $z = 0.45l$  and  $z = 0.55l$ , which is 14.9% for girders with 2 diaphragms and 17.8% with 5 diaphragms. Also, the error at the mid span for girders with 2 diaphragms is 13.3%. Thus shear strains of the cross section cannot be ignored when the transversal deformation of girders is considered.

5.2. Verifications with experiments

For further verification of the IPM, a series of experiments were performed using four groups of samples – girders with no diaphragms, one, two and three diaphragms, subjected to distortional loads. Diaphragms are equally distanced along the span. Both girders and diaphragms were fabricated from carbon structural steel plates (yield strength 235 MPa) of 8 mm thickness. All girders are

3 meters long, with height  $h = 0.6$  m and width  $b = 0.346$  m, giving a  $30^\circ$  angle between the diagonal and the web. All girders are sealed by a steel plate of 6 mm thickness on both ends.

To simultaneously produce two concentrated distortional loads, as in Fig. 4d, two steps were taken as follows

- (1) For distortional loads, as shown in Fig. 12, units were designed with two groups of wheels anti-symmetrically about the shear center  $O$  of the cross section. This is to decompose the horizontal power force  $P_{source}$  produced by FCS hydraulic servo system into two orthogonal loading components  $P_h$  and  $P_v$ .
- (2) For concentrated loads, as shown in Fig. 13, four stiff units of 1.5 m in length and 0.15 m and 0.350 m in width, respectively, were welded onto flanges and webs symmetrically over the mid span, and the loading sections were hence located at  $z_1 = 0.75$  m and  $z_2 = 2.25$  m, respectively.

During the experiments, compressive loadings were applied along the diagonal of the cross section by two anti-symmetrical wheel units, as shown in Fig. 12a. The entire experimental setup is shown in Fig. 14a, including two FCS hydraulic servo loading systems, two connection beams, two wheel units, four stiff units, the tested girder and two supports. The maximum loading was set to 5t with a loading speed of 2 mm/s, controlled by a loading equipment in Fig. 14b.

Fig. 15a shows measured points on the girder, with twelve equally distanced points  $A_1$ – $A_{11}$  on webs and  $B_1$ – $B_{11}$  on flanges. The transversal deformations on measured points were measured by dial gages, magnetically attached to a rectangular tube of

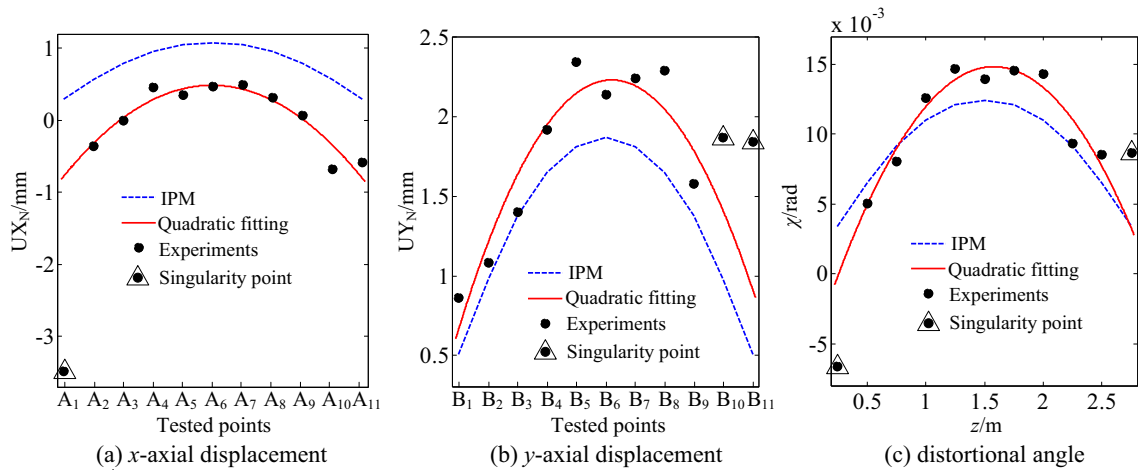


Fig. 16. Comparison of transversal displacements and angle between IPM and experiments under 5t loading.

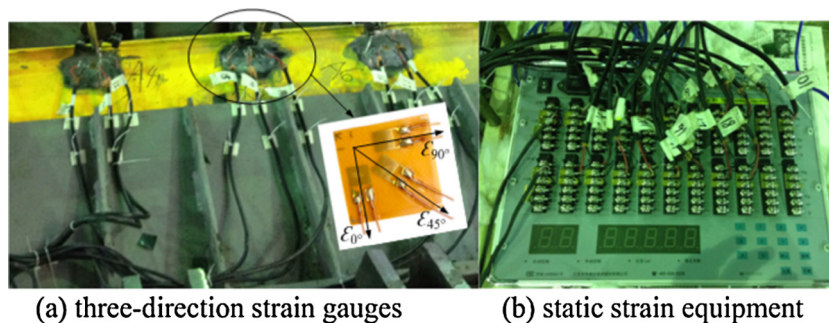


Fig. 17. Strain measurements.

3.5 m length, as shown in Fig. 15b. Measurements at each point gave the  $x$ - and  $y$ - axial deformations  $UX_N$  and  $UY_N$  ( $N = 1, \dots, 11$ ), and the distortional angle is calculated as

$$\chi(z) = \frac{2UX_N}{h} + \frac{2UY_N}{b} \quad (28)$$

Compared with those from IPM, the transversal displacements and distortional angle are depicted in Fig. 16 for girders without

diaphragms under the source loading of 5t. There exist some errors between the IPM and experimental results at the singularity points  $A_1$  for  $x$ -axial displacement and  $B_{10}$  and  $B_{11}$  for  $y$ -axial displacement, which are mainly caused by the residual strains of welding and manufacturing. Eliminating the influences induced by singularity points, fitting lines were obtained from experimental results by applying the quadratic fitting method provided in the software MATLAB. Fig. 16 shows reasonable agreements between two

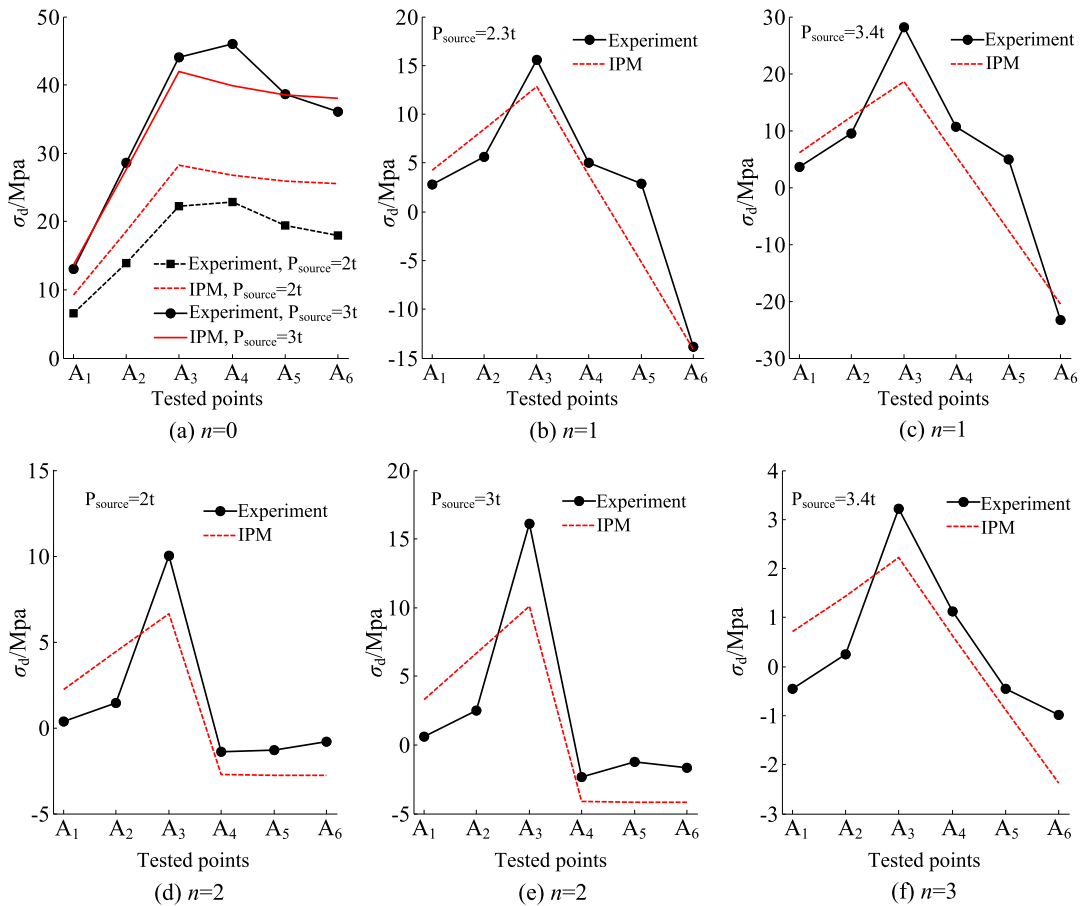


Fig. 18. Comparisons of distortional warping stresses between IPM and experiments ( $n$  being the total diaphragm number).

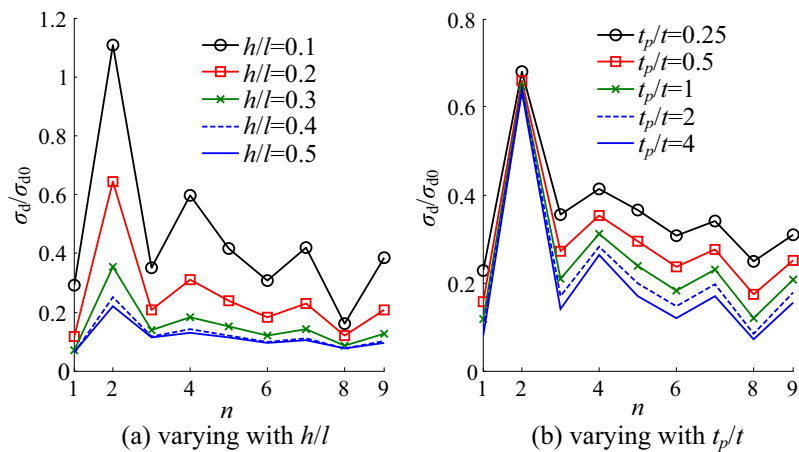


Fig. 19. The non-dimensional warping stress  $\sigma_d/\sigma_{d0}$ .

results. For distortional warping stresses, strains ( $\epsilon_{d-0^\circ}, \epsilon_{d-45^\circ}$  and  $\epsilon_{d-90^\circ}$ ) in three directions were measured at points A<sub>1</sub>–A<sub>6</sub> using strain gauges shown in Fig. 17a and recorded by the static strain equipment in Fig. 17b. The warping stress is calculated as

$$\sigma_d = \frac{E}{1-\nu^2} (\epsilon_{d-90^\circ} + \nu \epsilon_{d-0^\circ}) \quad (29)$$

where  $E = 2.1 \times 10^{11}$  Pa and  $\nu = 0.3$ .

Fig. 18 shows calculated distortional warping stresses on the tested points A<sub>1</sub>–A<sub>6</sub> for girders with (a) no diaphragm, (b, c) one diaphragm, (d, e) two diaphragms and (f) three diaphragms, respectively. It is seen that the warping stresses obtained from the IPM and experiments have the same up-and-down trend and with apices at A<sub>3</sub> for girders with diaphragms. The errors mainly come from the drop of  $\delta_h$  (Fig. 12a) between two horizontal source forces, which are mainly caused by the residual strain during manufacturing and welding. And this will produce torsional warping stress besides the distortional one.

### 6. Parametric study

In this section, the effects of the ratio of height to span of the girder  $h/l$ , the diaphragm thickness  $t_p$  and number  $n$  are examined on the distortion of simply supported girders with equally distanced inner diaphragms, where the loading and boundary conditions are referred to those in Section 5.1.

Fig. 19 shows the non-dimensional warping stress  $\sigma_d/\sigma_{d0}$  for node N at the loading section  $z = 0.45l$  varying with the ratios  $h/l$  and  $t_p/t$ , where  $\sigma_{d0}$  is the warping stress of girders without diaphragms. It is seen that except for the girder with two diaphragms under  $h/l = 0.1$ , the non-dimensional stress  $\sigma_d/\sigma_{d0}$  remains less than 1 and becomes smaller with the increment of  $n$ ,  $t_p/t$  and  $h/l$ , respectively. Besides, the  $\sigma_d/\sigma_{d0}$  decreases substantially when the number of diaphragm reduces from 2 to 1, or increases from 2 to 3, clearly indicating that the mid-span diaphragm plays a significant role in the reduction of distortional warping stress.

Fig. 20 shows the non-dimensional distortional angle  $\chi/\chi_0$  at the loading section  $z = 0.45l$  varying with  $h/l$  and  $t_p/t$ , where  $\chi_0$  is the distortional angle for girders without diaphragms. It is seen that except for the girder with two diaphragms under  $h/l = 0.1$ , the non-dimensional distortional angle  $\chi/\chi_0$  remains less than 0.25 and becomes smaller with the increment of  $n$ ,  $t_p/t$  and  $h/l$ , respectively. This implies that the inner diaphragms are capable of restraining the transversal deformation of the cross section, especially when  $n > 3$ . Similarly, compared with the distortional angle at  $n = 2$ , those at  $n = 1$  and 3 decrease significantly due to the restraint by the mid-span diaphragm.

Fig. 21 shows the non-dimensional warping displacement  $w_d/w_{d0}$  for node N at the loading section  $z = 0.45l$  varying with the ratios  $h/l$  and  $t_p/t$ , where  $w_{d0}$  is the warping displacement for girders without diaphragms. It is seen that except for the girder with two diaphragms under  $h/l = 0.1$ , the non-dimensional displacement

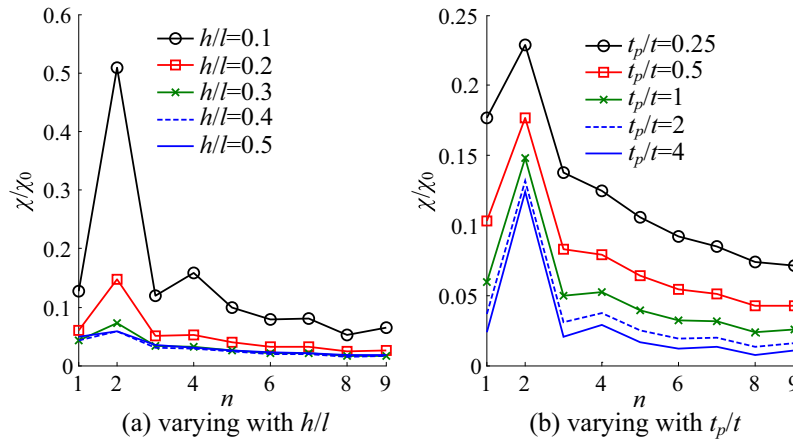


Fig. 20. The non-dimensional distortional angle  $\chi/\chi_0$ .

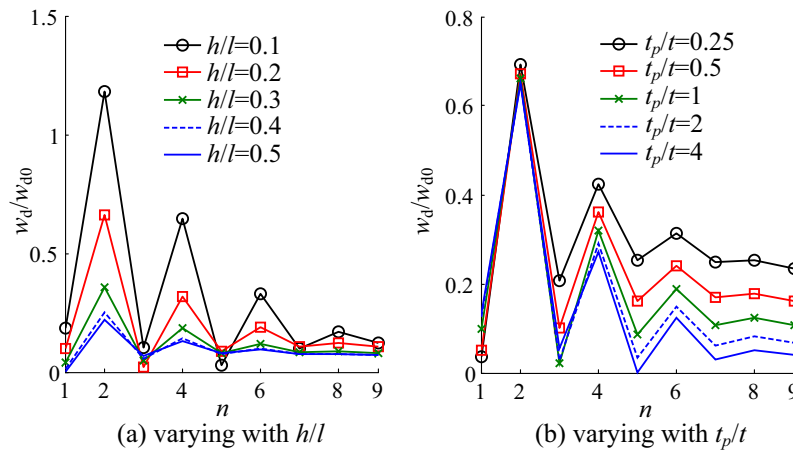


Fig. 21. The non-dimensional warping displacement  $w_d/w_{d0}$ .

ment  $w_d/w_{d0}$  in Fig. 21a remains less than 1.0 and converges to a fixed value between 0.1 and 0.2 for large diaphragm numbers.

**7. Buckling of both the local web plate and the mid-span diaphragm**

Taking a simply supported girder with uniform three inner diaphragms as an example, Fig. 22 shows 3D contours for the warping displacements and stresses, where the measurement, loading and boundary conditions are referred to those in Section 5.1. It is seen from Fig. 22 that the maximum displacement occurs at the local web plate at the loading sections, and the maximum stress occurs at the edge of the mid-span diaphragm, which may result in local buckling. It is thus necessary to check the stabilities for both local web plate and mid-span diaphragm.

In this section, the proposed IPM was carried to analyze the critical buckling values  $P_{cr1}$  and  $P_{cr2}$  for the eccentric load  $P_j$  according to the stabilities of the local web plate and the mid-span diaphragm, respectively. Inner diaphragms include one fixed

(diaphragm II) at the mid span and two (diaphragms I and III) symmetrical to the mid-span one. The loading and boundary conditions are referred to those in Section 5.1.

Fig. 23 shows the mixed stress boundary condition for the local web plate between the loading section and the mid span, in which  $a = 0.05l$ . Under distortional loads, the warping stress  $\sigma_d$  varies linearly from  $\sigma_{d1}$  at the loading section to  $\sigma_{d2} (= \beta\sigma_{d1})$  at the mid span and from  $\sigma_{d1(2)}$  on the top to  $-\sigma_{d1(2)}$  at the bottom. There also exists a constant shear stress  $\tau_{d1} (= \eta\sigma_{d1})$  on all four sides of the cross-section, and a parabola  $\tau_{d2}$  on both lateral sides. Both shear stresses can be obtained from [26]

$$\tau_d(s, z) = -\frac{M_d(z)}{I_t t} (S_d(s) - \frac{\int_F S_d(s) \rho_d(s) ds}{\int_F \rho_d(s) ds}) \quad (30)$$

where  $M_d(z)$  is the distortional moment in Fig. 2;  $I_t$  is the distortional warping constant in Eq. (1);  $t$  is the thickness of local web plate, given by  $t = 0.01$  m;  $F$  is the cross-sectional area;  $\rho_d(s)$  is the distance between the distortional center [6] and the mid line of the cross-sectional profile;  $S_d(s)$  is the second moment of area, given

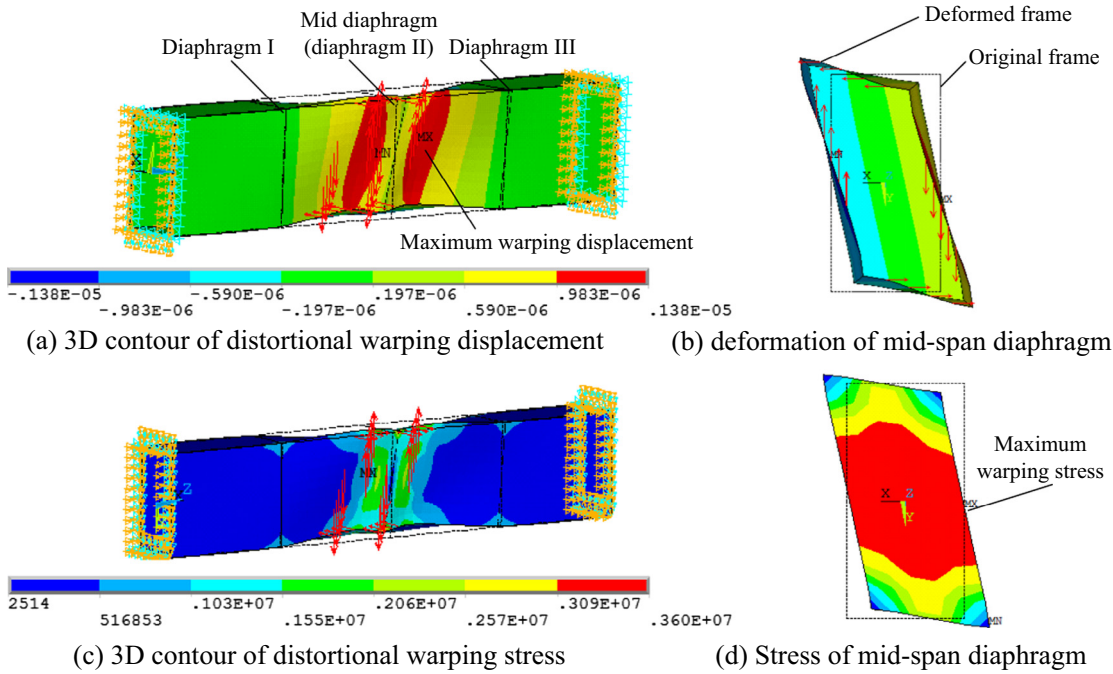


Fig. 22. 3D contours of warping displacement and stress of girders with three uniform inner diaphragms ( $t_p = 5$  mm).

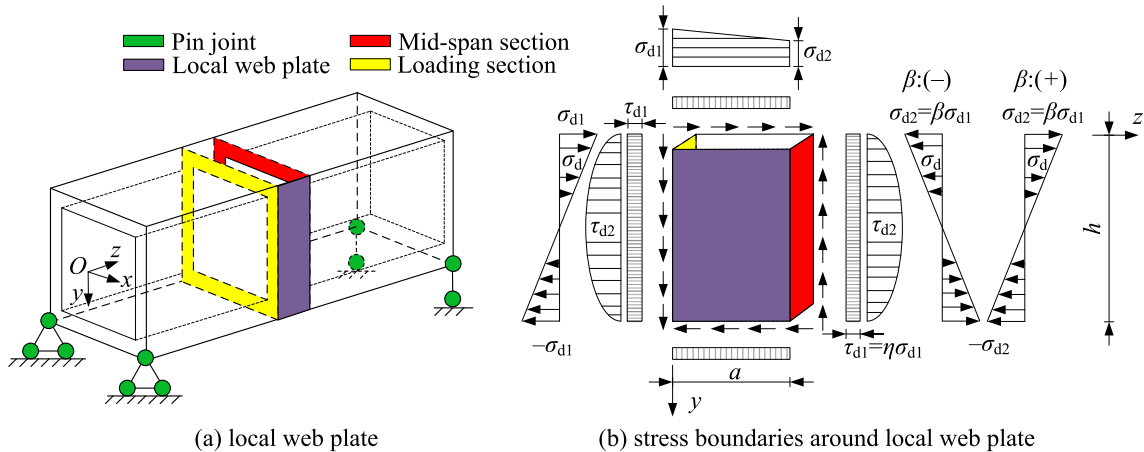


Fig. 23. Mixed stress boundaries of local web plate.

by  $S_d(s) = \int \hat{w} ds$ ,  $\hat{w}$  is the distortional sectorial coordinate [7],  $s$  is the circumferential coordinate around the cross-sectional profile.

Under the mixed stress boundary condition, the out-of-plane deformation  $w_p$  for local web plate can be indicated by the combination of two orthogonal sinusoidal functions in  $z$ - and  $y$ -axial directions, given by

$$w_p = \sum_{u=1}^{\infty} \sum_{v=1}^{\infty} A_{uv} \sin \frac{u\pi z}{a} \sin \frac{v\pi y}{h} \quad (31)$$

where  $u$  and  $v$  are the numbers of half waves in  $z$ - and  $y$ -axial directions;  $A_{uv}$  is the undetermined coefficient, which is the maximum of the combination of two sinusoidal functions.

For analysis, the distortional warping stress  $\sigma_d$  and the shear stress  $\tau_d$  for the local web plate can be presumed as [31]

$$\sigma_d = \sigma_{d1} \left(1 - \frac{2}{h}y\right) \left(1 - \frac{1-\beta}{a}z\right) \quad (32)$$

$$\tau_d = \tau_{d1} + \tau_{d2} = \sigma_{d1}\eta + \sigma_{d1} \frac{1-\beta}{a} \left(y - \frac{y^2}{h}\right) \quad (33)$$

where  $\beta$  is the ratio of the warping stresses  $\sigma_{d1}$  to the  $\sigma_{d2}$ ;  $\eta$  is the ratio of the warping stress  $\sigma_{d1}$  to the constant shear stress  $\tau_{d1}$ . Both ratios are calculated from IPM.

To obtain the critical buckling stress  $(\sigma_{d1})_{cr}$  for the local web plate, Galerkin equation [32] is applied, given by ( $p, q = 1, 2, \dots, \infty$ )

$$\int_0^a \int_0^h \left( \frac{\partial^4 w_p}{\partial z^4} + 2 \frac{\partial^4 w_p}{\partial z^2 \partial y^2} + \frac{\partial^4 w_p}{\partial y^4} + t\sigma_d \frac{\partial^2 w_p}{\partial z^2} + 2t\tau_d \frac{\partial^2 w_p}{\partial z \partial y} \right) \times \sin \frac{p\pi z}{a} \sin \frac{q\pi y}{h} dz dy = 0 \quad (34)$$

Substitute Eqs. (31)–(33) into Eq. (34), the latter is changed into

$$\sum_{u=1}^{\infty} \sum_{v=1}^{\infty} A_{uv} \left\{ \begin{aligned} & \left( \frac{u\pi}{a} \right)^2 + \left( \frac{v\pi}{h} \right)^2 \int_0^a \int_0^h \sin \frac{u\pi z}{a} \sin \frac{v\pi y}{h} \sin \frac{p\pi z}{a} \sin \frac{q\pi y}{h} dz dy \\ & - t\sigma_{d1} \left( \frac{u\pi}{a} \right)^2 \int_0^a \int_0^h \left(1 - \frac{2}{h}y\right) \left(1 - \frac{1-\beta}{a}z\right) \sin \frac{u\pi z}{a} \sin \frac{v\pi y}{h} \sin \frac{p\pi z}{a} \sin \frac{q\pi y}{h} dz dy \\ & + t\sigma_{d1} \frac{2u\pi v^2}{ah^2} \int_0^a \int_0^h \left[ \eta + \frac{1-\beta}{a} \left(y - \frac{y^2}{h}\right) \right] \cos \frac{u\pi z}{a} \cos \frac{v\pi y}{h} \sin \frac{p\pi z}{a} \sin \frac{q\pi y}{h} dz dy \end{aligned} \right\} = 0 \quad (35)$$

where the definite integrals on variables  $u$  and  $p$  are given in Table 1; and the integrals on  $v$  and  $q$  are obtained by replacing  $u$  and  $p$ .

Eq. (35) can be translated into a matrix equation set and the determinant of the coefficient matrix should be zero as the coefficient  $A_{uv}$  cannot be zero. Therefore, the critical stress  $(\sigma_{d1})_{cr}$  can be obtained.

In addition, since the dimension of the coefficient matrix affects the calculation accuracy, the critical stresses  $(\sigma_{d1})_{cr}$  were examined first in Fig. 24 under different dimensions of the coefficient matrix. In the calculation, the span  $l = 1$  m, the height  $h = 0.25$  m, the width  $b = 0.1$  m, the thicknesses for webs and flanges  $t = 0.01$  m, and the diaphragm thickness  $t_p = 0.005$  m. It is seen that the critical stress  $(\sigma_{d1})_{cr}$  tends to a converged value as the dimension of the coefficient matrix increases from  $2 \times 2$  to  $4 \times 4$ . However, calculation time increases significantly from 12 s to 51220 s. Considering both the accuracy and time, the  $3 \times 3$  coefficient matrix is regarded most appropriate to calculate the critical stress  $(\sigma_{d1})_{cr}$ .

In order to obtain  $P_{cr1}$ , a linear relationship is established between the critical moment  $M_{cr1}$  and the critical stress  $(\sigma_{d1})_{cr}$ .

$$\frac{M_{cr1}}{M_e} = \frac{(\sigma_{d1})_{cr}}{(\sigma_{d1})_e} \quad (36)$$

where  $M_{cr1}$  is the critical value for external moment  $M_j$  based on the stability of the local web plate, given by  $M_{cr1} = P_{cr1} \cdot n_1 / 2$ .  $M_e$  is the unit external moment, i.e.  $M_e = 1$  Nm.  $(\sigma_{d1})_e$  is the corresponding

**Table 1**  
Several definite integral items used in Eq. (35).

Definite integrals	$u = p$	$u \neq p$ and $u + p$ :even	$u \neq p$ and $u + p$ :odd
$\int_0^a \sin \frac{u\pi z}{a} \sin \frac{p\pi z}{a} dz$	$\frac{a}{2}$	0	0
$\int_0^a \cos \frac{u\pi z}{a} \sin \frac{p\pi z}{a} dz$	0	0	$\frac{-2ap}{\pi(u^2 - p^2)}$
$\int_0^a z \sin \frac{u\pi z}{a} \sin \frac{p\pi z}{a} dz$	$\frac{a^2}{4}$	0	$\frac{-4a^2 up}{\pi^2(u^2 - p^2)^2}$
$\int_0^a y \cos \frac{u\pi y}{a} \sin \frac{p\pi y}{a} dy$	$-\frac{a^2}{4u\pi}$	$\frac{pa^2}{\pi(u^2 - p^2)}$	$-\frac{pa^2}{\pi(u^2 - p^2)}$
$\int_0^a y^2 \cos \frac{u\pi y}{a} \sin \frac{p\pi y}{a} dy$	$-\frac{a^3}{4u\pi}$	$\frac{pa^3}{u(m^2 - p^2)}$	$\frac{4pa^3(3u^2 + p^2)}{\pi^2(u^2 - p^2)^3} - \frac{pa^3}{\pi(u^2 - p^2)}$

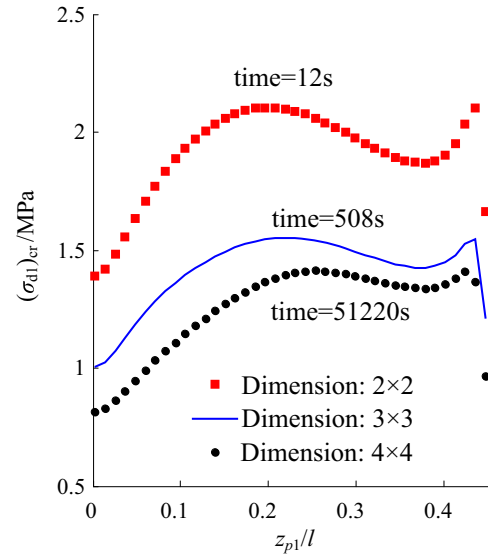


Fig. 24. Convergence of critical distortional warping stress  $(\sigma_{d1})_{cr}$ .

warping stress on top of the web at the loading section  $z = 0.45l$ , produced by the unit moment  $M_e$ .

Fig. 25 gives the critical load  $P_{cr1}$  varying with the location  $z_{p1}$  of diaphragm I for various ratios  $h/b$ , based on the stability of the local web plate. It is seen that the critical load  $P_{cr1}$  increases remarkably when diaphragm I is located close to the loading section  $z_1 = 0.45l$ , implying that installation of a diaphragm at the loading section will enhance effectively the stability of the local web plate.

While for the mid-span diaphragm (diaphragm II) subjected to pure shear boundary conditions, the critical value  $(M_{p2})_{cr}$  for moment  $M_{p2}$  is given by [33,34]

$$(M_{p2})_{cr} = \frac{E\pi^4 t_{p2}^3}{\xi(1 - \nu^2)}, \quad (h/b \leq 2)$$

$$(M_{p2})_{cr} = \left( \frac{89h}{200b} + \frac{b}{3h} \right) \frac{E\pi^2 t_{p2}^3}{1 - \nu^2}, \quad (h/b > 2) \quad (37)$$

where  $\xi = \frac{384b^2 h^2}{9(h^2 + b^2)^2} \sqrt{\frac{706}{625} + \frac{81}{25} \left( \frac{h^2 + b^2}{h^2 + 9b^2} \right)^2} + \frac{81}{25} \left( \frac{h^2 + b^2}{9h^2 + b^2} \right)^2$ ;  $\nu$  is the Poisson's ratio and equals to 0.3;  $t_{p2}$  is the thickness of mid-span diaphragm and  $t_{p2} = 0.005$  m.

Based on Eq. (21), the critical moment  $M_{cr2}$  for external moment  $M_j$  can be calculated by

$$M_{cr2} = - \frac{(M_{p2})_{cr}}{Q_{21} + Q_{22}} \quad (38)$$

where  $Q_{21}$  and  $Q_{22}$  are defined in Eq. (21).

Furthermore, based on equation  $M_j = P_j \cdot n_1 / 2$  [26], the critical load  $P_{cr2}$  can be finally obtained from Eq. (38). For the stability of the mid-span diaphragm, Fig. 26 gives the critical load  $P_{cr2}$  varying

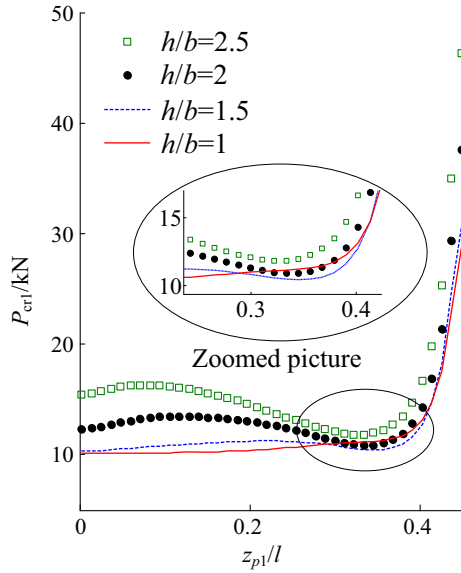


Fig. 25. The critical load  $P_{cr1}$  obtained from the stability of local web plate.

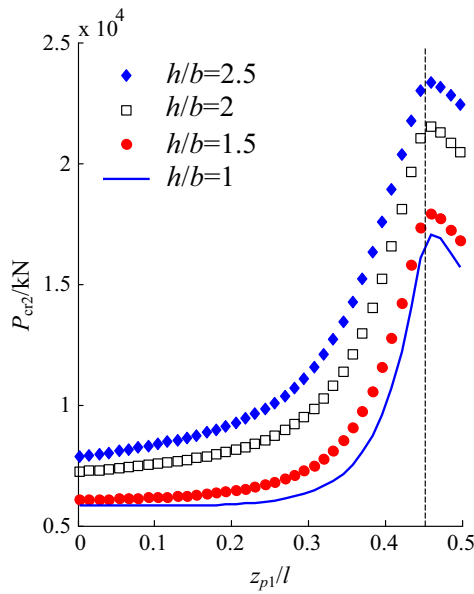


Fig. 26. The critical load  $P_{cr2}$  obtained from the stability of the mid diaphragm.

with the location  $z_{p1}$  of diaphragm I for various values of  $h/b$ . It is seen that the critical load  $P_{cr2}$  increases remarkably when diaphragm I is located close to the loading section  $z_1 = 0.45l$ , indicating increased resistance to buckling.

Back to the girder with equally-distanced three inner diaphragms in Fig. 22, the girder will reach its yield strength limit of 235 MPa when the eccentric load  $P_j$  is 650 kN, which is much smaller than the critical buckling load  $P_{cr2}$  of 8743 kN at  $z_{p1}/l = 0.25$  for the ratio  $h/b = 2$  according to the stability of the mid-span diaphragm. Simultaneously, the plastic yield load of 650 kN is much larger than the critical load  $P_{cr1}$  of 12.2 kN at  $z_{p1}/l = 0.25$  according to the stability of the local web plate. This implies that buckling of the local web plate will be the primary failure mode with the increment of eccentric loads  $P_j$ . Hence attentions should be paid on the stability of the local web plate for the design of girders subjected to eccentric loads.

## 8. Conclusions

In this paper, the initial parameter method (IPM) is applied to investigate the distortion of simply supported girders with inner diaphragms subjected to concentrated eccentric loads, where in-plane shear deformation of diaphragms is considered. The main conclusions can be drawn as follows

- (1) Compared with results from FEA and experiments, accurate analyses can be obtained by IPM for the distortional angle, warping displacements and stresses for simply supported girders with inner diaphragms. Both the in-plane shear deformation of diaphragms and the compatibility condition between the girder and diaphragms are taken into account in IPM. Besides, comparison of results between considering the shear strain of the cross section and not shows that the shear strain of the cross section cannot be ignored when calculating the distortional angle.
- (2) Both the distortional angle and warping stresses decrease with the increment of the ratio of height to span, the number of diaphragms and their thickness. The warping displacement converges to a fixed value between 0.1 and 0.2 for large diaphragm numbers. And the mid-span diaphragm plays a key role in reducing the distortional deformations and stresses under symmetrical loads.
- (3) Stabilities of the local web plate and the mid-span diaphragm were both investigated for box girders with symmetrical three inner diaphragms. Results show that both the local web plate and the mid-span diaphragm increase their resistance to buckling when the diaphragm I is located close to the loading sections. Moreover, the local web plate will buckle first as the primary failure mode. Therefore, attentions are needed on the stabilities of the local web plate for simply supported girders under eccentric loads.

Based on the IPM, it is possible to improve the warping displacements and stresses of simply supported girders through optimizing the positions and wall thickness of diaphragms. Future work are needed for (1) optimization of the distortion of girders with diaphragms; (2) mechanical properties of girders with perforated diaphragms.

## Acknowledgements

This work was supported by the National Natural Science Foundation of China (NSFC) [grant number: 51175442 and 51675450].

## Appendix A

The relationships between  $\varphi_i(z)$  ( $i = 1, 2, 3, 4$ ) and their differentiations is

$$\begin{aligned} \varphi_1' &= \lambda_1 \varphi_4 + \lambda_2 \varphi_2, \quad \varphi_2' = \lambda_1 \varphi_3 - \lambda_2 \varphi_1, \quad \varphi_3' = \lambda_1 \varphi_2 - \lambda_2 \varphi_4, \quad \varphi_4' \\ &= \lambda_1 \varphi_1 + \lambda_2 \varphi_3; \end{aligned} \quad (A1)$$

$$\begin{aligned} \varphi_1'' &= (\lambda_1^2 - \lambda_2^2) \varphi_1 + 2\lambda_1 \lambda_2 \varphi_3, \quad \varphi_2'' = (\lambda_1^2 - \lambda_2^2) \varphi_2 - 2\lambda_1 \lambda_2 \varphi_4, \\ \varphi_3'' &= (\lambda_1^2 - \lambda_2^2) \varphi_3 - 2\lambda_1 \lambda_2 \varphi_1, \quad \varphi_4'' = (\lambda_1^2 - \lambda_2^2) \varphi_4 + 2\lambda_1 \lambda_2 \varphi_2; \end{aligned} \quad (A2)$$

$$\begin{aligned} \varphi_1''' &= (\lambda_1^3 - 3\lambda_1 \lambda_2^2) \varphi_4 + (3\lambda_1^2 \lambda_2 - \lambda_2^3) \varphi_2, \quad \varphi_2''' = (\lambda_1^3 - 3\lambda_1 \lambda_2^2) \varphi_3 - (3\lambda_1^2 \lambda_2 - \lambda_2^3) \varphi_1, \\ \varphi_3''' &= (\lambda_1^3 - 3\lambda_1 \lambda_2^2) \varphi_2 - (3\lambda_1^2 \lambda_2 - \lambda_2^3) \varphi_4, \quad \varphi_4''' = (\lambda_1^3 - 3\lambda_1 \lambda_2^2) \varphi_1 + (3\lambda_1^2 \lambda_2 - \lambda_2^3) \varphi_3. \end{aligned} \quad (A3)$$

## References

- [1] Pezeshky P, Mohareb M. Distortional theory for the analysis of wide flange steel beam. *Eng Struct* 2014;75:181–96.
- [2] Senjanovic I, Fan Y. On torsional and warping stiffness of thin-walled girders. *Thin-Walled Struct* 1991;11:233–76.
- [3] Alghamdi SA. Static and modal analysis of twin-cell box girder structures. *AIAA J* 2001;39:1406–10.
- [4] Zhang H, Desroches R, Yang ZJ, et al. Experimental and analytical studies on a streamlined steel box girder. *J Constr Steel Res* 2010;66:906–14.
- [5] Dabrowski R. Curved thin-walled girders theory and analysis. Cement and Concrete Association, 1968.
- [6] Boswell LF, Li Q. Consideration of the relationships between torsion, distortion and warping of thin-walled beams. *Thin-Walled Struct* 1995;21:147–61.
- [7] Li Q. Investigation of the warping functions of thin walled bars with closed cross section. *J Southwest Jiaotong Univ* 1993;6:1–6.
- [8] Wright RN, Abdel-Samad SR, Robinson AR. BEF analogy for analysis of box-girders. *J Struct Div* 1968;94:1719–43.
- [9] Hsu YT, Schelling DR. EBEF method for distortional analysis of steel box-girder bridges. *J Struct Eng* 1995;121:557–66.
- [10] Hsu YT, Fu CC. Application of EBEF method for the distortional analysis of steel box girder bridge superstructures during construction. *Adv Struct Eng* 2002;5:211–21.
- [11] Zhao ZM, Fang ZZ, Guo JQ. Analysis of continuous box girders with diaphragms by finite strip method. *Bridge Constr* 1993;4:35–53.
- [12] Cheung YK. Finite strip method in structural analysis. Oxford: Pergamon Press; 1976.
- [13] Zhao ZM. The calculating analysis for multiple span continuous curved box girder by the finite strip method. *J Fuzhou Univ (N Sci)* 1997;25:90–4.
- [14] Zhao ZM. Analysis of continuous curved box-girder bridge with flexible transverse diaphragms by finite strip method. *Comp Struct Mech Appl* 1993;10:473–84.
- [15] Suetake Y, Hirashima M. Extended trigonometric series analysis of box girders with diaphragms. *J Eng Mech*. 1997;123:293–301.
- [16] Park N, Lim N, Kang Y. A consideration on intermediate diaphragm spacing in steel box girder bridges with a doubly symmetric section. *Eng Struct* 2003;25:1665–74.
- [17] Park N, Choi Y, Yi G, et al. Distortional analysis of steel box girders. *Steel Struct* 2002;2:51–8.
- [18] Park N, Choi S, Kang Y. Exact distortional behavior and practical distortional analysis of multicell box girders using an expanded method. *Comp Struct* 2005;83:1607–26.
- [19] Park N, Kang YJ, Kim HJ. An independent distortional analysis method of thin-walled multicell box girders. *Struct Eng Mech* 2005;21:275–93.
- [20] Park N, Choi Y, Kang Y. Spacing of intermediate diaphragms in horizontally curved steel box girder bridges. *Finite Elem Anal Des* 2005;41:925–43.
- [21] Zhang L. Influences of diaphragm plate and geometric characteristics on distortion effect of steel box girder. *J Railway Eng Soc* 2013;8:68–73.
- [22] Li HF, Luo YF. Application of stiffness matrix of a beam element considering section distortion effect. *J Southeast Univ* 2010;26:431–5.
- [23] Vlasov VZ. Thin walled elastic beams, 2nd ed. Jerusalem, Israel. Available from Office of Technical Services, US Department of Commerce, Washington, D.C.: Israel Program for Scientific Translations; 1961.
- [24] Xu X, Qiang SZ. Research on distortion analysis theory of thin-walled box girder. *Eng Mech* 2013;30:192–201.
- [25] Xu X, Ye HW, Qiang SZ. Distortional analysis of thin-walled box girder taking account of shear deformation. *Chin J Comp Mech* 2013;30:860–6.
- [26] Harashima M, Usugi K. Distortional analysis of random box girders considering the shear deformation. *Foreign Bridge* 1980;1:1–29.
- [27] Sakai F, Okumura T. Influence of diaphragms on behaviour of box girders with deformable cross section. *Intl Assoc Bridge Struct Eng* 1972;9:285–98.
- [28] Oleinik JC, Heins CP. Diaphragms for curved box beam bridges. *J Struct Div, ASCE* 1975;101:2161–78.
- [29] Park N, Kang YJ. Distortional analysis of multicell box girders using 3-dimensional shell elements-I. Proposal and application of an expanded method. *J Korean Soc Civ Eng A* 2004;24:557–63.
- [30] Park N, Kang YJ. Distortional analysis of multicell box girders using 3-dimensional shell elements-II. Distortional analysis based on the expanded method. *J Korean Soc Civ Eng A* 2004;24:565–72.
- [31] Lu YZ. Buckling of simply-supported rectangular plates under combined actions of shear and bending stresses varying linearly in longitudinal direction. *J Tongji Univ* 1991;19:481–7.
- [32] Fletcher CA. Computational Galerkin methods. Berlin: Springer-Verlag, Berlin Heidelberg; 1984.
- [33] Liu HW, Lin JX, Cao ML. The theory of plates and shells. China: Zhejiang University Press; 1987.
- [34] Xiao MX. The stability of plates. China: Sichuan Science and Technology Press; 1993.